Meningeal IL-17 producing T cells mediate cognitive impairment in salt-sensitive hypertension

Monica M. Santisteban[1]
Samantha Schaeffer[1]
Antoine Anfray[1]
Giuseppe Faraco[1]
David Brea Lopez[1]
Gang Wang[1]
Melissa Sobanko[1]
Rose Sciortino[1]
Gianfranco Racchumi[1]
Ari Waisman[2]
Laibaik Park[1]
Josef Anrather[1]
Costantino Iadecola[1]

[1]Feil Family Brain and Mind Research Institute
Weill Cornell Medicine
New York, NY 10065, USA

[2]Institute for Molecular Medicine
University Medical Center,
Mainz, Germany

Correspondence:
Costantino Iadecola, MD
ORCID: 0000-0001-9797-073X
coi2001@med.cornell.edu

Monica M. Santisteban, PhD*
ORCID: 0000-0002-2836-9075
mms2012@med.cornell.edu
Present address: monica.santisteban@vumc.org

Feil Family Brain and Mind Research Institute
Weill Cornell Medicine
407 E 61st Street
New York, NY 10065
Phone: 646-962-8279

Word Count: 14,604

Short running title: Meningeal IL-17 and cognitive impairment

NONSTANDARD ABBREVIATIONS

Ach: acetylcholine

Ang II: angiotensin II

ASL: arterial spin label

AT1R: ang II type 1 receptor

BAM: brain associated macrophages

bECKO: brain endothelial cell knockout

BM: bone marrow

BP: blood pressure

CBF: cerebral blood flow

DOCA: deoxycorticosterone acetate

eNOS: endothelial nitric oxide synthase

HTN: hypertension

i.c.v.: intracerebroventricular

IL-17: interleukin 17

IL-17RA: IL-17 receptor A

KO: knockout

NO: nitric oxide

RAS: renin angiotensin system

ROS: reactive oxygen species

Th17: T-helper 17

WT: wild-type

ABSTRACT

Hypertension, a disease afflicting over one billion individuals worldwide, is a leading cause of cognitive impairment, the mechanisms of which remain poorly understood. In a mouse model of hypertension, we found that the neurovascular and cognitive dysfunction depends on IL-17, a cytokine elevated in hypertensive individuals. However, neither circulating IL-17 or brain angiotensin signaling could account in full for the dysfunction. Rather, IL-17 produced by T-cells in the dura mater was the major culprit by reaching the cerebrospinal fluid and activating IL-17 receptors on brain associated macrophages. Accordingly, depleting brain macrophages, deleting IL17-RA in brain macrophages, or suppressing meningeal T cells completely rescued cognitive function without attenuating blood pressure elevation, circulating IL-17 or brain angiotensin signaling. The data unveil a critical role of meningeal T-cells and macrophage IL-17 signaling in the neurovascular and cognitive dysfunction of hypertension and suggest novel therapies to counteract the devastating effects of hypertension on cognitive health.

INTRODUCTION

Hypertension (HTN) is a major cause of death and disability worldwide, and a leading risk factor for dementia[1]. Although there have been significant advances in the pharmacotherapy, a sizable proportion of patients have uncontrolled or resistant HTN which is particularly damaging to the brain[2, 3]. Furthermore, despite suggestive evidence that a rigorous control of blood pressure (BP) may lower the risk of mild cognitive impairment[4], the burden of HTN on the brain remains substantial, including a 10% risk of recurrent cerebrovascular events despite BP control and no proven strategy to prevent dementia[5]. Therefore, there is need to gain a deeper understanding the damaging effects of HTN on the brain and to develop new approaches to protect cognitive health. Dysfunction of vital cerebrovascular regulatory mechanisms, such as the ability of neural activity to adjust the delivery of cerebral blood flow (CBF; functional hyperemia) or the regulation of microvascular perfusion by endothelial cells, have been strongly implicated in the deleterious effects of HTN on the brain[6]. However, the cellular and molecular basis through which the factors involved in BP elevation drive the neurovascular dysfunction associated with cognitive impairment remain poorly understood.

Salt-sensitivity is a critical factor in essential HTN[7], affecting approximately 50% of hypertensive individuals[8]. Experimental studies using the deoxycorticosterone acetate (DOCA)-salt model have provided evidence that the renin-angiotensin system (RAS) is activated in brain and suppressed in the periphery[9, 10]. Indeed, a large proportion of individuals with resistant HTN, particularly African American and women, exhibit low levels of circulating renin, a key protease needed for angiotensin II (Ang II) production, suggesting suppression of systemic RAS[11, 12]. It is also well established that HTN induces immune dysregulation and elevates circulating levels of the cytokine interleukin (IL)-17 both in animals and humans[13-15]. Interestingly, high dietary salt increases circulating levels of IL-17 by promoting polarization of T-helper 17 lymphocytes (Th17) in the gut and induces neurovascular dysfunction and cognitive impairment[16-18].

105 However, the role IL-17 in the deleterious effects of salt-sensitive HTN on cognitive function, its
106 sources and targets, and its relationships with brain RAS remain unexplored.
107 Here, we used the DOCA-salt model to examine the role of IL-17 in the neurovascular
108 and cognitive dysfunction associated with salt-sensitive HTN. We found that DOCA-salt HTN
109 alters key homeostatic mechanisms controlling the cerebral blood supply and leads to cognitive
110 impairment. These deleterious effects are not driven by central Ang II signaling, but are
111 associated with IL-17 signaling on both sides of the blood-brain barrier (BBB). In the circulation,
112 IL-17 derived from gut and circulating T-cells activates IL-17 receptors A (IL-17RA) on cerebral
113 endothelial cells to impair their ability to regulate cerebral perfusion, but this mechanism does
114 not explain in full the cognitive deficits. On the brain side, unexpectedly, IL-17 derived from T-
115 cells in the dura mater acts on IL-17RA on brain-associated macrophages (BAM)[19, 20] to induce
116 neurovascular uncoupling and cognitive impairment. Accordingly, depletion of meningeal T-cells
117 or BAM completely rescues the cognitive phenotype. These findings unveil a previously
118 unappreciated critical involvement of meningeal T-cells and IL-17 in the cognitive impairment
119 associated with salt sensitive HTN and suggest novel approaches to ameliorate the deleterious
120 impact of HTN on cognitive function.
121
122 RESULTS
123 Salt-sensitive HTN induces neurovascular and cognitive impairment linked to expansion of IL-
124 17-producing cells
125 First, we sought to examine the impact of HTN on neurovascular and cognitive function. To this
126 end, we used the DOCA-salt model of salt-sensitive HTN, in which mice are implanted with a
127 s.c. pellet of DOCA and receive 0.9% NaCl in the drinking water[9, 21]. DOCA-salt treatment
128 evoked a sustained elevation of BP beginning 3 days after pellet implantation (Fig 1A). An
129 increase in circulating sodium was observed at 21 days (Suppl table 1), but the sodium content
130 did not increase in brain, kidney and small intestine (Suppl Fig 1A). However, as previously

131 reported in mouse models and in individuals with refractory HTN[22], skin sodium content was
132 increased without changes in potassium (Suppl Fig 1B). To examine the neurovascular effects
133 of DOCA-salt HTN, we assessed CBF by laser-Doppler flowmetry in anesthetized mice with a
134 cranial window overlying the somatosensory cortex under close monitoring of key physiological
135 variables (Fig 1B; Methods)[23, 24]. DOCA-salt attenuated the increase in CBF evoked by neural
136 activity induced by mechanical stimulation of the facial whiskers (functional hyperemia; Fig 1B-
137 D), as well as the increase in CBF produced by bathing the somatosensory cortex with
138 acetylcholine (ACh; Fig 1E), a response dependent on endothelial nitric oxide (NO)[25]. Both
139 responses were impaired starting at day 10 after DOCA. However, smooth muscle vasoactivity,
140 tested by neocortical application of adenosine (Fig 1F), BBB permeability to low molecular
141 weight dextran (Suppl Fig 2A-B), and resting CBF (ml/100g/min) assessed by arterial spin label
142 (ASL)-MRI (Suppl Fig 2C-D) were not impaired at day 21 after DOCA, indicating that the
143 suppression of functional hyperemia and endothelial vasodilatation did not result from
144 widespread neurovascular damage. DOCA-salt also altered cognitive function, as demonstrated
145 by a reduction in the mice ability to discriminate between familiar and novel objects (working
146 memory) (Fig 1G), a reduction of time spent in the target quadrant during the Barnes Maze
147 probe trial (spatial learning and memory) (Fig 1H), and impaired nest building ability (activities of
148 daily living) (Fig 1I). Representative images from each group are shown for each of these
149 cognitive tasks (Fig 1G-I). Importantly, the neurovascular alterations preceded the development
150 of cognitive impairment (Fig 1D, E, G), an observation consistent with a mechanistic link
151 between neurovascular dysfunction and cognitive impairment[26].

152 Based on the emerging role of IL-17 in human HTN[13-15, 27, 28] and in dietary salt-induced
153 cognitive impairment[24], we then examined whether IL-17 contributes to the neurovascular and
154 cognitive effects of DOCA-salt HTN. Circulating IL-17 increased gradually over the course of the
155 DOCA-salt treatment (Fig 2A), beginning at day 10 when neurovascular dysfunction first
156 became apparent (Fig 1D-E). Focusing on the gut, an organ enriched with IL-17-producing

157 cells[29], we observed that 21 days of DOCA-salt increased *Il17a* mRNA expression (Fig 2B). To
158 identify the cellular sources of IL-17, we induced DOCA-salt HTN in mice carrying the gene
159 encoding eGFP at the *Il17a* locus[30] and observed increased IL17-GFP+ cells at 21 days (Fig
160 2C-D) in the small intestine lamina propria, identified by flow cytometry to be Th17 and γδT17
161 cells (Fig 2E-G, Suppl Fig 3). Th17 and γδT17 cells have been shown to enter the circulation[30,
162 31], and they were also increased in blood and spleen in DOCA-salt (Fig 2H-I), as in patients with
163 HTN in whom circulating IL17-producing cells are increased[27, 28]. We found no evidence of IL-17
164 production by neutrophils (Suppl. Fig 4).
165 To test whether IL-17 contributes to the deleterious effects of salt-sensitive HTN, we
166 induced DOCA-salt HTN in IL-17 deficient mice (IL17KO; Fig 2J, Suppl table 2). IL17KO mice
167 developed an increase in BP and circulating sodium similar to wild-type (WT) mice (Suppl Fig
168 5A, Suppl Table 1), but did not exhibit an attenuation in functional hyperemia and endothelial
169 vasodilation (Fig 2K-L). Furthermore, no deficits were observed in either novel object or Barnes
170 maze tests (Fig 2M-N). Thus, IL-17 produced by Th17 and γδT17 cells is essential for the
171 neurovascular and cognitive dysfunction in DOCA-salt HTN.
172
173 <u>IL-17 impairs endothelial vasodilation by downregulating NO bioavailability via endothelial IL-17</u>
174 <u>receptors</u>
175 Next, we sought to identify the cellular targets of the IL-17 contributing to neurovascular and
176 cognitive impairment. Since endothelial cells are in direct contact with circulating IL-17, which is
177 elevated in DOCA salt HTN (Fig 2A), we first assessed the contribution of cerebral endothelial
178 IL-17RA. To this end, we deleted brain endothelial IL-17RA by administering an adeno-
179 associated virus expressing Cre recombinase in cerebral endothelial cells (AAV-BR1-iCre;
180 i.v.)[32, 33] to IL-17RA$^{flox/flox}$ mice[34], referred to as IL-17RA^{bECKO}. AAV-BR1-iCre delivery in Ai14-
181 ROSA^{tdTomato} reporter mice (Suppl Fig 6A) demonstrated widespread endothelial cell

182 transduction in the cerebral microvasculature (Suppl Fig 6B). Most importantly, we observed 90-
183 95% endothelial viral transduction in vessels less than 20μm (Suppl Fig 6C-D), which include
184 the arterioles involved in CBF regulation[35] . Three weeks after AAV-BR1-iCre delivery in IL-
185 17RA$^{flox/flox}$, we observed a reduction in *Il17ra* genomic DNA in sorted brain endothelial cells but
186 not in microglia (Supp Fig 6E-F), consistent with the selectivity of this viral vector[33, 36]. IL-
187 17RA^{bECKO} mice (Fig 3A) had increases in BP and circulating IL-17 comparable to those of
188 DOCA-salt WT mice (Suppl Fig 5B, Suppl table 2), but the CBF response to ACh was
189 completely rescued (Fig 3B). However, no improvement was observed in functional hyperemia
190 (Fig 3C). Since the IL-17 has been shown to suppress endothelial NO production by inducing
191 inhibitory eNOS phosphorylation at Thr^{495} [24], we also examined NO production and endothelial
192 nitric oxide synthase (eNOS) phosphorylation in DOCA-salt treated mice. Resting and ACh-
193 induced endothelial NO production was attenuated in DOCA cerebral microvascular
194 preparations (Fig 3D), an effect associated with an increase in eNOS inhibitory phosphorylation
195 (Fig 3E). However, as predicted by the rescue of endothelial vasoactivity (Fig 3B), the increase
196 in eNOS Thr^{495} phosphorylation was suppressed in IL-17RA^{bECKO} DOCA-salt mice (Fig 3F),
197 attesting to the link between endothelial IL-17RA and eNOS inhibitory phosphorylation.
198 Consistent with the partial rescue in neurovascular function, IL-17RA^{bECKO} DOCA-salt mice
199 displayed cognitive improvement only at novel object recognition, not the Barnes maze (Fig 3G-
200 H).
201
202 <u>BAM contribute to the neurovascular and cognitive dysfunction in DOCA-salt HTN</u>
203 Cerebral endothelial IL-17RA knockdown ameliorated the neurovascular and cognitive function
204 only partially, while total IL17KO rescued the dysfunction in full, suggesting the involvement of
205 IL-17RA on other vessel-associated cell types. BAM, including perivascular and leptomeningeal
206 macrophages, express IL-17RA[37] and have been implicated in models of neurovascular and
207 cognitive dysfunction[23, 38], raising the possibility that they may also play a role DOCA-salt HTN.

208 To test this hypothesis, we examined the effect of BAM depletion via intracerebroventricular
209 (i.c.v.) delivery of liposome-encapsulated clodronate (Fig 4A)[23, 38]. Liposomes containing vehicle
210 (PBS) or clodronate were injected i.c.v. on the same day as DOCA-salt treatment was started.
211 This protocol depleted 80% of perivascular and leptomeningeal BAM (Fig 4B-C) within the time-
212 frame of the experiment[23], without affecting microglia or blood leukocytes[23], BBB permeability[33],
213 or neurovascular function[23, 38]. Dural macrophages were depleted initially but, unlike the
214 leptomeningeal and perivascular BAM, were fully restored within 21 days (Suppl Fig 7A-B). The
215 BP (Suppl Fig 5C) and serum IL-17 (Suppl table 2) increases evoked by DOCA-salt were not
216 affected by clodronate treatment. However, BAM depletion completely normalized functional
217 hyperemia (Fig 4D), and partially improved endothelial vasoactivity (Fig 4E). Additionally, BAM
218 depletion improved cognitive function as assessed by novel object recognition and Barnes maze
219 (Fig 4F-G). These observations demonstrate that BAM contribute to the deleterious
220 neurovascular and cognitive effects of DOCA-salt HTN.
221
222 <u>BAM contribute to neurovascular and cognitive dysfunction through IL17RA-dependent ROS</u>
223 <u>production</u>
224 Due to their myeloid origin, BAM are enriched with the ROS producing enzyme Nox2 and are
225 major source of vascular oxidative stress[23, 39, 40]. Neocortical application of the ROS scavenger
226 MnTBAP rescued the impairment of functional hyperemia in DOCA-salt (Fig 4H), attesting to the
227 involvement of ROS in the neurovascular dysfunction. Therefore, we sought to determine if
228 DOCA-salt increases ROS production in BAM and, based on the results in IL17KO mice (Fig 2J-
229 N), whether the effect is IL-17 dependent. Dissociated brain cells from WT control and DOCA-
230 salt mice were incubated with the ROS probe dihydroethidium (DHE; Fig 4I) and stained for
231 identification of BAM ($CD45^{hi}CD11b^{+}CD36^{+}$; Suppl Fig 8A,D)[23, 41], microglia ($CD45^{int}CD11b^{+}$)[33,
232 42], and endothelial cells ($CD45^{-}Ly6C^{+}$)[33, 42] using flow cytometry[23, 33, 41, 42]. We found that DOCA-
233 salt increased ROS production in BAM, but not in microglia or endothelial cells (Fig 4J). DOCA-

234 salt failed to increase ROS in BAM of IL-17RA deficient mice (Fig 4K), indicating that IL-17
235 signaling is needed for BAM ROS production in DOCA-salt HTN. Consistent with this
236 conclusion, recombinant IL-17 (10ng/mL) increased ROS production in BAM, as assessed with
237 two different probes (Fig 4L).

238 To provide further evidence that IL-17RA in BAM are involved, we used a bone marrow
239 (BM) chimera-based approach. We and others have demonstrated that BM transplantation after
240 total body irradiation repopulates leptomeningeal and perivascular compartments with BM-
241 derived macrophages[23, 33, 43, 44]. Therefore, we transplanted IL-17RA$^{-/-}$ or Nox2$^{-/-}$ BM into WT
242 mice to replace BAM with IL-17RA$^{-/-}$ or Nox2$^{-/-}$ BM-derived cells (Fig 4M). Three months later,
243 mice were placed on the DOCA-salt protocol. WT mice transplanted with WT BM (WT→WT)
244 exhibited alterations in CBF responses and cognition identical to those observed in naïve mice
245 (Fig 4N-Q, Fig 1D-H), indicating that although BAM in these mice are derived from the BM, they
246 are pathogenically equivalent to native yolk sac-derived BAM[23, 38]. Deletion of either IL-17RA or
247 Nox2 in BAM prevented the impairment of functional hyperemia in full (Fig 4N) and partially
248 improved endothelial vasoactivity (Fig 4O), as observed in the BAM depletion experiments (Fig
249 4D-E). Additionally, IL-17RA$^{-/-}$→ WT and Nox2$^{-/-}$→ WT chimeras showed improved cognitive
250 function (Fig 4P-Q). Attesting to the requirement of IL-17RA in BAM, ROS production was
251 blunted in BAM from IL-17RA$^{-/-}$→ WT DOCA-salt chimeras (Suppl Fig 9B). Since ROS are a
252 well-known product of IL17 signaling[45] these data also provide evidence of IL17RA activation in
253 BAM.

254 To complement the BM chimera data implicating IL17RA in BAM, we developed a novel
255 mouse expressing tamoxifen-inducible Cre recombinase under the control of the Mrc1 promoter
256 (Mrc1$^{CreERT2/+}$; Fig. 5A). First, we sought to determine whether Mrc1^{CreERT2} heterozygosity altered
257 BAM number and distribution across brain compartments (Suppl Fig 10A). To this end, after
258 labeling BAM by i.c.v. injection of FITC dextran (Suppl Fig 10B), we confirmed that the number
259 of BAM in dural, pial, and perivascular spaces of Mrc1$^{CreERT2/+}$ mice were not different from those

260 in Mrc1$^{+/+}$ (WT) mice (Suppl Fig 10C-G). Next, to characterize the efficiency of this novel Cre
261 driver mouse, we crossed Mrc1^{CreERT2} with Ai14 TdTM (Fig 5B-C). Following tamoxifen
262 treatment, we found widespread TdTM expression in pial and perivascular BAM (Suppl Fig 11A-
263 F). TdTM was not detected in Iba1+ microglia (Suppl Fig 11E). Tamoxifen treatment of adult
264 Mrc1$^{CreERT2/+}$ crossed with IL17-RA$^{flox/flox}$ (BAM$^{IL17RA-/-}$) led to a 78.9% reduction in IL17-RA+ BAM
265 (Fig 5D-E, Suppl Fig 11G-H), without affecting the BP response (Fig 5F) and circulating IL-17
266 elevation (Suppl Table 2) induced by DOCA-salt. Consistent with the findings in IL-17RA$^{-/-}$→ WT
267 chimeras, we observed full rescue of functional hyperemia without improvement of endothelial
268 vasodilation (Fig. 5G-H). Additionally, BAM$^{IL17RA-/-}$ DOCA-salt mice showed improved cognitive
269 function (Fig 5I-J). Collectively, the findings with BM chimera, and our novel Mrc1$^{CreERT2/+}$ mouse
270 provide converging evidence that IL-17RA in BAM are critical for the alterations in functional
271 hyperemia and cognitive function induced by DOCA-salt HTN.
272
273 <u>DOCA-salt HTN increases IL-17-producing T cells in the dura mater</u>
274 Next, we sought to define the cellular source(s) of IL-17 acting on BAM IL-17RA to induce
275 neurovascular and cognitive dysfunction. Recent evidence indicates that IL-17-producing T cells
276 are present in the dura mater[46, 47], and are able to modulate rodent behavior[48, 49]. In agreement
277 with these findings, *Il17a* mRNA was detected in the dura of control mice and was markedly
278 increased by 21 days of DOCA-salt treatment (Fig 6A). *Il17a* mRNA was not observed in the
279 brain parenchyma (Fig 6A). To map IL-17 producing cells in brain and dura we used IL17-GFP
280 reporter mice. Consistent with the mRNA data, IL17-GFP+ cells were not observed in the brain
281 (Suppl Fig 12), but were found in the dura (Fig 6B-D), as previously reported[48, 50]. DOCA-salt
282 treatment (21 days) led to a significant increase in IL17-GFP+ cells surrounding the venous
283 sinuses but not in regions removed from the sinus (Fig 6B-C). To determine whether these cells
284 actually secrete IL-17, we performed an IL-17 ELISpot assay to detect cytokine release with
285 single-cell resolution[51] in isolated dural leukocytes. We found that dural cells secrete IL-17, and

286 this response is increased in DOCA-salt mice (Fig 6E-F). We then used flow cytometry to
287 characterize the IL17-GFP+ cells. We did not observe an increase of CD45+ immune cells in
288 the dura of DOCA-salt mice (Fig 6G). We found no change in the total number of CD4 or Th17,
289 (Suppl Fig 13A-B), or the percent of CD4 producing IL-17 (Fig 6H), excluding a role for these
290 cells. There was no change in the total number of total γδT cells (Suppl Fig 13C) and a trend
291 towards increase of γδT17 cells (Suppl Fig 13D). Interestingly, we observed an increase in the
292 percentage of γδT cells producing IL17 (Fig 6I). Since the total number of γδT-cells did not
293 change (Suppl Fig 13C), changes in other cells populations would not impact the % of γδTcells
294 producing IL17. Therefore, consistent with data in the literature[48], we observed an increased in
295 the proportion of dural γδT cells producing IL17. The increase in dural IL-17 production after 21
296 days of DOCA-salt was associated with increased detection of IL-17 in the cerebrospinal fluid
297 (CSF; Fig 6J). To gain insight on how dura-derived IL-17 reaches the CSF, we assessed the
298 structural integrity of the arachnoid barrier using immunocytochemistry for the arachnoid barrier
299 tight junction marker claudin-11[52]. We found significant tight junction remodeling in DOCA-salt
300 mice as evidenced by (1) discontinuous tight junctions (Fig 6K), (2) reduced arachnoid domain
301 areas (Fig 6L-M), and (3) altered tight junction morphology (Fig 6K)[53, 54]. Collectively, these
302 findings suggest that IL-17 generated by T-cells in the dura reach the CSF in the subarachnoid
303 space via a disrupted arachnoid barrier and engage IL-17RA on BAM. Of note, we did not
304 observe changes in key inflammatory genes (Suppl Fig 14A-B) or evidence of microglia and
305 astrocyte activation (Suppl Fig 14C-D), suggesting that dura-derived IL17 did not result in a
306 massive neuroinflammatory reaction which could potentially contribute to cognitive impairment
307 in DOCA-salt.
308
309 <u>Cognitive impairment in salt-sensitive HTN is driven by dural IL17-producing γδT cells</u>

310 Next, we sought to provide evidence in support of the involvement of dural IL17-producing cells
311 in the neurovascular and cognitive effects of DOCA salt HTN. Dural γδT cells, like other γδT
312 cells[55], are tissue resident, with only 1-2% being derived from the circulation under
313 homeostasis[48]. However, in inflammatory conditions, an increased influx of γδT cells into lymph
314 nodes and subsequent homing to inflamed tissues via the circulation has been shown[56, 57].
315 Given that circulating Th17 and γδT17 cells are both elevated in DOCA-salt, it is conceivable
316 that T cells migrate from the circulation to the dura. To test this hypothesis, we utilized FTY720
317 (fingolimod), a sphingosine-1-phosphate receptor (S1PR) modulator that depletes circulating
318 lymphocytes, including γδT17 and Th17 cells, by preventing their egress from lymphoid tissues
319 and gut, as well as other mechanisms[31, 58-61]. FTY720 (1mg/kg i.p. every 3 days[24]) was
320 administered from day 7 through day 21 of DOCA-salt treatment (Fig 7A) and did not affect the
321 development of HTN (Fig 7B). As expected, FTY720 significantly reduced circulating $CD4^+$ T
322 cells (Fig 7C) without affecting the elevation in circulating IL-17 in DOCA-salt mice (Fig 7D).
323 FTY720 depleted IL17-GFP+ cells in the dura (Fig 7E), both Th17 cells (Fig 7F), and γδT17 cells
324 (Fig 7G). Interestingly, FTY720 did not ameliorate the CBF response evoked from the
325 endothelium (Fig 7H), attesting to its dependence on circulating IL-17 acting on cerebral
326 endothelial IL-17RA and not BAM. The reduction of IL-17 producing T cells in the dura was
327 associated with full rescue of functional hyperemia (Fig 7I) and improved of cognitive function
328 (Fig 7J-K), as well as suppression of ROS production in BAM (Suppl Fig 9C).
329 To confirm the role of dural γδT cells in the neurovascular and cognitive dysfunction in
330 DOCA-salt, we infused anti-TCRγδ antibody into the cerebral ventricles (i.c.v.) using osmotic
331 minipumps from day 7 through day 21 of DOCA-salt treatment (Fig 7L) to deplete γδT cells in
332 the dura (Fig 7M). i.c.v. delivery of this antibody has been previously shown to decrease γδT
333 cell production of IL-17 in the dura[48], but did not affect the BP response to DOCA-salt (Fig 7N).
334 Consistent with results of the FTY720 experiments, γδT cell-depletion in the dura did not

335 improve endothelial vasodilation (Fig 7O). The reduction of γδT cells in the dura rescued
336 functional hyperemia (Fig 7P), and improved cognitive function (Fig 7Q-R). Thus, dural IL17-
337 producing T-cells are the source of the IL-17 contributing to the neurovascular and cognitive
338 impairment in salt-sensitive HTN.
339
340 The contribution of Ang II to the cerebrovascular dysfunction in DOCA-salt depends on IL-17
341 signaling
342 It is well established that the DOCA-salt treatment leads to activation of brain RAS[9, 10], which
343 has been implicated in endothelial dysfunction in large and small cerebral vessels[62]. In apparent
344 contrast, our data suggest that IL-17 is essential for the neurovascular and cognitive dysfunction
345 in DOCA-salt HTN. Therefore, we investigated the relationship between brain Ang II and IL-17
346 in this model. As expected, DOCA-salt treatment elevated Ang II levels in brain and reduced it in
347 the circulation (Fig 8A-B). These effects were associated with mRNA upregulation of brain Ang
348 II receptors type 1A (AT1R) (*Agtr1a*; Fig 8C*)* and downregulation of kidney renin (*Ren1*; Fig 8D),
349 confirming activation of RAS in brain and suppression in the periphery[62]. Central AT1R blockade
350 by i.c.v. infusion of losartan (Fig 8E), prevented the increase in BP caused by DOCA-salt[9]
351 (Suppl Fig 5) but did not attenuate the increase in circulating IL-17 (Suppl table 2). Accordingly,
352 i.c.v. losartan restored functional hyperemia (Fig 8F), but did not improve endothelium-
353 dependent vasodilation (Fig 8G), consistent with circulating IL-17 being the predominant
354 mediator of the endothelial dysfunction. Central AT1R blockade ameliorated cognitive
355 impairment only partially, with an improvement observed only in novel object recognition, but not
356 at the Barnes maze (Fig 8H-I). Since Ang II induces ROS production in BAM leading to
357 neurovascular dysfunction[23], we wondered if IL-17 signaling in BAM is required for Ang II-
358 induced ROS production. Ang II stimulation increased ROS production in WT but not IL17RA$^{-/-}$
359 BAM (Fig 8J). However, indices of brain RAS activation were not attenuated in IL17KO mice
360 (Suppl Fig 15A) or mice in which dural production of IL-17 was suppressed by treatment with

361 FTY720 (Suppl Fig 15B), suggesting that brain RAS activation in the absence of dural IL-17 is
362 not sufficient to induce neurovascular dysfunction. In support of this conclusion, bathing the
363 cerebral cortex with Ang II to activate AT1R on BAM[23], induced neurovascular dysfunction in
364 WT but not IL17KO mice (Fig 8K-L). Thus, IL-17 signaling is necessary for the contribution of
365 Ang II to the neurovascular and cognitive impairment of salt-sensitive HTN.
366

367 DISCUSSION

368 We have demonstrated that the neurovascular and cognitive dysfunction associated with salt-
369 sensitive HTN is mediated by two distinct mechanisms involving IL-17 signaling in cerebral
370 endothelium and BAM (Suppl Fig 16): (1) in the circulation, IL-17 produced by T-cells acts on
371 cerebral endothelial IL-17RA to reduce NO production leading to suppression of endothelial
372 vasoactivity without affecting the increase in CBF induced by neural activity; (2) in the brain, IL-
373 17 produced by dura T-cells acts on IL-17RA on BAM to induce vascular oxidative stress and
374 suppression of functional hyperemia with minimal effects on endothelial function. However,
375 these two mechanisms do not contribute equally to the cognitive dysfunction: counteracting the
376 effect of circulating IL-17 by endothelial IL-17RA deletion rescues cognition only partially, while
377 counteracting the sources (T-cells) or targets of central IL-17 (BAM or BAM IL-17RA) rescues
378 cognitive function in full. Furthermore, endothelial NO synthase phosphorylation is not involved
379 in the mechanisms of neurovascular coupling since functional hyperemia can be rescued
380 completely by BAM depletion or IL17RA deletion in BAM despite persistent endothelial
381 vasomotor dysfunction. Thus, the deleterious effects of BAM on functional hyperemia cannot be
382 attributed to endothelial dysfunction or eNOS phosphorylation. Therefore, the data unveils an
383 unanticipated central role of meningeal T-cells in the deleterious cognitive effect of salt sensitive
384 hypertension.

385 There is increasing evidence that inflammation and immunity participate in the
386 pathobiology of HTN[63]. Pioneering studies have unveiled a role of innate and adaptive immunity

387 in the central and peripheral mechanisms driving the elevation in BP and on the end organ
388 damage, particularly in the kidney and the vasculature[64-66]. In this context, T-cells and IL-17
389 have emerged as important mediators of the effect of Ang II and DOCA-salt HTN on peripheral
390 organs and vessels, in part verified in hypertensive patients[67]. Here, we extend these
391 observations by providing evidence that dural T-cells and IL-17 play a critical role in the
392 neurovascular and cognitive deficits in a model of HTN reproducing key attributes of the human
393 disease[10, 68]. While the dura mater has recently been recognized as major players in the
394 immune responses of the brain underling brain injury and repair[46, 48], our findings provide insight
395 into an previously unrecognized pathogenic role of meningeal immunity in HTN. Our studies
396 revealed that the dura is the critical site of the immune responses underlying the neurovascular
397 and cognitive deficits in HTN. This process is driven by a crosstalk between dural T-cells and
398 BAM through IL-17 signaling. Thus, depletion of IL-17-producing T-cells in the dura, depletion of
399 BAM or deletion of IL-17RA on BAM, rescues the cognitive deficits in full. As for the
400 mechanisms by which BAM alter neurovascular coupling, evidence from our studies implicate
401 Ang II[23] and amyloid-beta[38] inducing BAM production of ROS, which are thought to inactivate
402 neuronal NO and other vasoactive mediators released from neurons and converging on
403 resistance arteriole to mediate vasodilatation[35, 69].

404 The DOCA salt model is associated with increases in brain RAS signaling and reduction
405 of the systemic RAS[10], which we have verified by central and peripheral measurements of Ang
406 II. DOCA salt HTN is well established to induce alterations in cerebral vascular regulation both
407 in vivo and in isolated cerebral arteries and arterioles[21, 62]. Surprisingly, however, our study
408 showed that the vascular effects of Ang II, mediated by ROS production by BAM, require IL-17.
409 Thus, ex vivo Ang II is unable to increase ROS production in BAM in the absence of IL-17RA,
410 and in vivo Ang II applied to the neocortex to target meningeal and perivascular BAM does not
411 induce neurovascular dysfunction IL17KO mice. These observations unveil a critical
412 requirement of IL-17 in the deleterious effects of Ang II. Considering the key role that Ang II and

413 IL-17 signaling play in health and disease the molecular basis of their interaction is of great
414 interest and will require further exploration.

415 Owing to the absolute reliance of the brain on the delivery of blood flow, reduced
416 cerebral perfusion or alterations in neurovascular regulation have long been implicated in
417 cognitive impairment induced by vascular factors as well as Alzheimer's disease[70, 71]. Our
418 studies, in general, support a link between CBF regulation and cognitive health, but they also
419 suggest effects of IL-17 independent of blood flow. While resting CBF is not reduced, blocking
420 cerebral endothelial IL-17 signaling rescues endothelial vasoactivity and produces partial
421 cognitive improvement. On the other hand, counteracting central Ang II signaling rescues only
422 neurovascular coupling and leads to a partial improvement in cognition. Although it is
423 conceivable that endothelial dysfunction and neurovascular uncoupling could play an additive
424 role in the cognitive deficits, this possibility seems unlikely because depletion of dural T-cells
425 provides complete cognitive rescue while improving only neurovascular coupling and not
426 endothelial function. Direct effects of IL-17 on neurons have been demonstrated in other
427 models[48, 49, 72, 73], which in conjunction with the vascular effects could contribute to the cognitive
428 dysfunction.

429 It is well established that HTN is a leading risk factor for cognitive impairment caused
430 both by vascular factors and neurodegeneration[6], but the evidence that antihypertensive
431 therapy reduces such risk is inconsistent and limited[74, 75]. Our findings reveal an additional layer
432 of complexity in the deleterious effects of HTN on the brain and suggest new preventive and
433 therapeutic approaches. The central actions of Ang II are critical for the development of HTN by
434 inducing neurohumoral dysfunction. This aspect was highlighted by our observation that central
435 inhibition of AT1R prevented the BP elevation completely but did not rescue the cognitive
436 dysfunction in full. While BP control remains critical for attenuating hypertensive end-organ
437 damage to kidney, heart, and vasculature[76], full protection of the brain may require also
438 targeting meningeal immunity. Considering the diversity of mechanisms underlying human

439 HTN[77], efforts to select hypertensive patients in which immune factors are involved, may identify
440 individuals at greater risk for the deleterious effects of dural immune signaling on the brain.
441 Since the infectious complications of suppressing immune signaling is a well-known concern in
442 patients with cardiovascular diseases[78], strategies to selectively target dural immunity would be
443 required[79].
444
445 MATERIALS AND METHODS
446 The data that support the findings of this study are available from the corresponding authors
447 upon request. Details on antibodies used and specific primer sequences are found in the Online
448 Supplement. For rigor and reproducibility, experiments were repeated at least twice throughout
449 the manuscript, and figures present pooled data.
450
451 *Experimental mouse models*
452 All procedures were approved by the Institutional Animal Care and Use Committee of Weill
453 Cornell Medicine and performed in accordance with the National Institutes of Health (NIH)
454 Guide for the Care and Use of Laboratory Animals. Studies were performed in a blinded fashion
455 in male C57BL/6 mice (WT, age 3-5 months, weight 25-30g; JAX, the Jackson Laboratory), IL-
456 17 GFP reporter mice (C57BL/6-*IL17a*^{tm1Bcgen}/J, JAX strain# 018472), IL-17 knockout mice
457 (*IL17a*$^{tm1.1(icre)Stck}$/J, JAX strain# 016879), and IL-17RA$^{flox/flox}$ mice[34]. IL-17RA$^{flox/flox}$ mice were
458 crossed with the germ-cell driven Sox2-Cre mice (B6.Cg-*Edil3*$^{Tg(Sox2\text{-}cre)1Amc}$/J, JAX strain#
459 008454)[80] to generate whole-body IL-17RA knockout mice. Bone marrow chimera experiments
460 detailed below were performed on C57BL/6 mice receiving donor cells from IL-17RA knockout
461 mice or B6.129S-*Cybb*^{tm1Din}/J mice (*Nox2*$^{-/-}$, JAX strain# 002365), both lines are congenic for
462 C57BL/6. AAV-BR1-iCre experiments detailed below were performed on B6.Cg-
463 *Gt(ROSA)26Sor*$^{tm14(CAG\text{-}tdTomato)Hze}$/J (Ai14 TdTomato reporter, JAX strain# 007914), and
464 homozygous IL-17RA$^{flox/flox}$ mice. Mrc1^{CreERT2} mice were generated by Cyagen. The Mrc1

465 targeting construct was linearized by restriction digestion with NotI, followed by
466 phenol/chloroform extraction and ethanol precipitation. The linearized vector was transfected
467 into C57BL/6 ES cells according to Cyagen's standard electroporation procedures. The
468 transfected ES cells were subject to G418 selection (200 μg/mL) 24 hours post electroporation.
469 179 G418 resistant clones were picked and amplified in 96-well plates. Two copies of 96-well
470 plates were made, one copy was frozen down and stored at -80°C and the other copy of the 96-
471 well plates was used for DNA isolation and subsequence PCR screening for homologous
472 recombination. The PCR screening identified 18 potential targeted clones, from among which 6
473 were expanded and further characterized by Southern blot analysis. Five of the six expanded
474 clones were confirmed to be correctly targeted.
475
476 The Mrc1 gene (NCBI Reference Sequence: NM_008625.2) is located on mouse chromosome
477 2. Thirty exons have been identified, with the ATG start codon in exon 1 and the TAG stop
478 codon in exon 30. In the targeting vector, the coding region of exon 1 plus part of intron 1 was
479 replaced with the CreERT2-polyA cassette. Correct integration of the CreERT2-polyA cassette
480 was confirmed by diagnostic PCR. Sequencing of the genomic region of interest after
481 amplification by PCR was further used to verify correct integration. After germline transmission,
482 correctly targeted founders were crossed with C57BL/6J mice to establish the colonies for this
483 study. Adult 6-10 week old mice were treated with tamoxifen citrate (Sigma: T-5648; oral
484 gavage; 200mg/kg) once a day for 5 consecutive days. Female mice were not included in this
485 study, as previous studies have shown that they have a blunted hypertensive and immune
486 response to DOCA-salt[81].
487
488 *DOCA-salt HTN*
489 Mice were randomized to treatment group and anesthetized by isoflurane inhalation for
490 subcutaneous implantation of a 50 mg pellet of DOCA (Innovative Research of America, Cat#

491 M-121) or sham surgery of equal duration[21]. After recovery from anesthesia, DOCA animals
492 were maintained on standard chow and *ad libitum* access to 0.9% NaCl in autoclaved tap water.
493 Control animals were maintained on standard chow and *ad libitum* access to autoclaved tap
494 water. Systolic BP was monitored in awake mice using tail-cuff plethysmography (Hatteras)[23, 33].
495 Mice were acclimated to tail-cuff plethysmography for one week prior to pellet or sham surgery,
496 and systolic BP was monitored twice a week after initiation of DOCA-salt.
497
498 *Tissue sodium measurement*
499 Mice were anesthetized with isoflurane, and blood was collected through cardiac puncture.
500 Brain, kidney, skin (dorsal abdomen), and distal small intestine (distal 10 cm) were isolated,
501 flash frozen, and stored at -80°C until analysis. After 15 minutes, blood was centrifuged at
502 2,000*g* for 15 minutes and serum was separated and stored at -80°C until analysis. The serum
503 renal chemical panel was performed by the Laboratory of Comparative Pathology (LCP) of Weill
504 Cornell Medicine Research Animal Resource Center, and the tissue mineral panel for sodium
505 measurement was performed by the Animal Health Diagnostic Center Toxicology Lab of Cornell
506 University Veterinary Medicine using inductively coupled plasma – atomic emission
507 spectrometry (ICP-AES)[82, 83].
508
509 *General surgical procedures for CBF studies*
510 Mice were anesthetized with isoflurane (induction, 5%; maintenance, 2%) and artificially
511 ventilated with a mixture of N_2 and O_2. One of the femoral arteries was cannulated for recording
512 mean arterial pressure (MAP) and collecting blood samples. Rectal temperature was maintained
513 at 37°C. After surgery, isoflurane was discontinued and anesthesia was maintained with
514 urethane (750 mg/kg, i.p.) and chloralose (50 mg/kg, i.p.). Throughout the experiment, the level
515 of anesthesia was monitored by testing of motor responses to tail pinch. Arterial blood gases

516 were monitored at the beginning and end of the experiment and maintained at pO_2 100-
517 110mmHg, pCO2 30-40mmHg, and pH 7.3-7.4[23]. As in previous studies[84], MAP remained within
518 the autoregulated range for CBF (Control: 82.77 ± 0.85 mmHg; DOCA: 106.37 ± 0.99 mmHg;
519 $p<0.05$). Due to the anesthesia, the baseline BP and the increase in BP induced by DOCA-salt
520 was lower than that observed in awake mice[9].
521
522 *Experimental protocol for experiments monitoring CBF reactivity*
523 As previously performed[23, 24, 38], a small craniotomy (2 × 2 mm) was performed to expose the
524 parietal cortex, the dura was removed, and the site was superfused with Ringer's solution
525 (37°C; pH 7.3–7.4)[23]. CBF was continuously monitored at the site of superfusion with a laser-
526 Doppler probe (Perimed) positioned stereotaxically on the cortical surface and connected to a
527 data acquisition system (PowerLab). CBF values were expressed as percentage increases
528 relative to the resting level. After MAP and blood gases were stable, CBF responses were
529 recorded. The whisker-barrel cortex was activated for 60 seconds by stroking of the
530 contralateral vibrissae, and the evoked changes in CBF were recorded. ACh (10 μM; Sigma-
531 Aldrich) or adenosine (400 μM; Sigma-Aldrich) was superfused on the exposed neocortex for 5
532 minutes[23, 24, 38]. In some experiments, CBF responses were tested before and after 30 minutes
533 of superfusion with the ROS scavenger MnTBAP (100μM)[23, 84] or Ang II (500nM)[23, 85].
534
535 *BBB permeability*
536 BBB permeability was assessed using fluorescein-dextran (FITC-dextran, MW 3kDa; 100μl of
537 1% solution i.v.), as previously described[23, 33]. The tracer was allowed to circulate for 20
538 minutes, and then mice were transcardially perfused with cold PBS to clear the intravascular
539 tracer. Brains were removed and olfactory bulb, brainstem, and cerebellum were discarded.
540 Samples were weighed and frozen on dry ice and stored at −80 °C until analysis. Tissue was
541 homogenized in 400μL of PBS, mixed with 400μL of methanol, and centrifuged at 13,000*g* for

542 30 minutes. The supernatant was used for measurement of the amount of FITC-dextran (485nm
543 excitation and 530 nm emission), measured in duplicate using a fluorescence
544 spectrophotometer, together with standards, and normalized to brain tissue weight.
545
546 *Measurement of resting CBF by ASL-MRI*
547 CBF was assessed quantitatively using arterial spin labeling magnetic resonance imaging (ASL-
548 MRI) at 21 days of DOCA-salt, performed on a 7.0-tesla 70/30 Bruker Biospec small-animal MRI
549 system with 450 mT/m gradient amplitude and a 4,500 $T \cdot m^{-1} \cdot s^{-1}$ slew rate. A volume coil was
550 used for transmission and a surface coil for reception. Anatomical localizer images were
551 acquired to find the transversal slice approximately corresponding to bregma +0.5 mm. This
552 position was used for subsequent ASL-MRI, which was based on a flow-sensitive alternating
553 inversion recovery rapid acquisition with relaxation enhancement (FAIR-RARE) pulse sequence
554 labeling the inflowing blood by global inversion of the equilibrium magnetization. One axial slice
555 was acquired with a field of view of 15 × 15 mm, spatial resolution of 0.117 × 0.117 × 1 mm, TE
556 (echo time) of 5.368 ms, effective TE of 48.32 ms, recovery time of 10 s, and a RARE (rapid
557 imaging with refocused echoes) factor of 72. Twenty-two turbo inversion recovery values
558 ranging from 30 to 2,300 ms were used, and the inversion slab thickness was 4 mm. For
559 computation of resting CBF (rCBF), the Bruker ASL perfusion processing macro was used. It
560 uses a published model[86] and includes steps to mask out the background. The masked rCBF
561 images were exported to Analyze format on the MRI console. The ASL images were analyzed
562 by ImageJ and the average CBF value is reported in mL per 100 g of tissue per min[24].
563
564 *Novel object recognition test*
565 The novel object recognition test (NOR) task was conducted in a plastic box measuring 29 cm ×
566 47 cm × 30 cm high[23, 24]. Stimuli consisted of plastic objects that varied in color and shape, but
567 had similar size. A video camera was used to record the testing session for offline analysis

568 using AnyMaze software. Mice were acclimated to the testing room for 1 hour each day prior to
569 the start of each day. On day 1, mice were acclimated to the testing chamber (habituation). On
570 day 2, mice were placed in the same chamber in the presence of 2 identical sample objects and
571 were allowed to explore for 5 minutes. After an intersession interval of 1 hour, mice were placed
572 in the same chamber, but 1 of the 2 objects was replaced by a novel object. Mice were allowed
573 to explore for 5 minutes. Between trials, the maze is cleaned with 10% ethanol in water to
574 minimize olfactory cues. Exploratory behavior was assessed manually by two experimenters
575 blinded to the treatment group. Exploration of an object was defined as the mouse sniffing the
576 object or touching the object while looking at it[23]. A minimal exploration time for both objects
577 (total exploration time) during the test phase (5 seconds) was used. The amount of time taken to
578 explore the novel object was expressed as percentage of the total exploration time and provides
579 an index of working memory.
580
581 *Barnes Maze*
582 As described previously[23, 24], we used a Barnes maze consisting of a circular open surface (90
583 cm in diameter) elevated to 90cm by four wooden legs. There are 20 circular holes (5 cm in
584 diameter) equally spaced around the perimeter, positioned 2.5cm from the edge of the maze.
585 No wall or intra-maze visual cues are placed around the edge. A plastic escape box (11 x 6 x 5
586 cm) was positioned beneath one of the holes. Mouse movement is tracked with the Any-Maze
587 software (Stoelting). Mice are tested in groups of 10, and between trials are placed into cages in
588 a dark room adjacent to the test room for the intertrial interval (45 minutes). Mice are habituated
589 to the dark room for 60 min prior to the start of each day. No habituation trial is performed. The
590 acquisition phase consists of three consecutive training days with three 3-minute trials per day
591 with the escape hole located at the same location across trials and days. On each trial, a mouse
592 is placed into a start tube located in the center of the maze, the start tube is raised, and the
593 buzzer is turned on until the mouse enters the escape hole. After each trial, mice remain in the

594 escape box for 60s before being returned to their home cage. Between trials, the maze is
595 cleaned with 10% ethanol in water to minimize olfactory cues. Three parameters of learning
596 performance are recorded: (1) latency to locate the escape hole, (2) distance traveled before
597 locating the escape hole, and (3) number of errors made. Errors are defined as head-pokes into
598 non-escape holes and are counted manually. On the fourth day, the probe trial is performed and
599 consists of a 1.5 min trial where the escape hole has been removed. The memory parameter
600 recorded is percent of time spent in the target quadrant where the escape hole used to be.
601
602 *Nest building*
603 The ability of mice to build nests is assessed by the Deacon rating scale[24, 87]. 1 hour prior to the
604 dark cycle, each mouse is placed in a new clean cage containing 5g of nestlet (Ancare) in the
605 middle of the cage. Food, water, and lighting parameters are not changed from standard
606 housing practices. The next day, nests are assessed on a rating scale of 1-5[87], and untorn
607 nestlet pieces are weight. The cognitive parameters recorded are (1) nest score, and (2) percent
608 of untorn nestlet.
609
610 *IL-17 measurement*
611 IL-17 concentration in serum was measured by cytometric bead array mouse IL-17A Enhanced
612 Sensitivity Flex Set (BDBiosciences)[24] or by electrochemiluminescence-based multi-array MSD
613 V-Plex Mouse IL-17A Kit (MesoScale)[88], according to the manufacturer's instructions.
614
615 *Immunofluorescence*
616 IL17-eGFP and wild-type mice were anesthetized with sodium pentobarbital (120 mg/kg, i.p.)
617 and perfused transcardially with phosphate-buffered saline (PBS) followed by 4%
618 paraformaldehyde (PFA) in PBS. Distal small intestine, brain, and skull cap were removed and
619 post-fixed overnight in 4% PFA. Small intestine was then submerged in 30% sucrose solution

620 for 3 days, frozen, and sections (thickness: 30 μm) were cut through the whole distal small
621 intestine using a cryostat and then place on a slide. Free-floating coronal brain sections
622 (thickness 40 μm) were cut through the whole brain using a vibrating microtome. Dura whole
623 mounts were prepared by careful stripping from the skull cap using fine surgical forceps, as has
624 been previously described by us[24, 30, 89] and others[48, 50, 90]. For leptomeningeal mounting, PFA-
625 perfused brains were post-fixed in methanol on a shaker at room temperature for 10 minutes[52].
626 Then, the leptomeninges were carefully stripped from the surface of the brain, and mounted on
627 slides for staining[52-54]. Brain sections and dura whole mounts were permeabilized in 0.5%
628 Triton-PBS and then blocked with 5% of normal donkey or goat serum in 0.1% Triton-PBS.
629 Sections were incubated with primary antibodies (Suppl Table 3) at 4°C overnight in 2% normal
630 donkey or goat serum in 0.1% Triton-PBS. Leptomeningeal mounts were blocked with 5%
631 normal donkey or goat serum and 5% BSA in 0.1% Triton-PBS. Sections were then incubated
632 with species-specific secondary antibody (1:100, Jackson ImmunoResearch whole IgG affinity-
633 purified antibodies) and mounted on slides with VectaShield Hardset mounting medium with
634 DAPI (Vector Labs), visualized with a laser-scanning confocal microscope (Leica TCS SP8),
635 and analyzed on ImageJ software by an investigator blinded to the treatment groups. IL17-GFP
636 cells in the dura were analyzed as sinus-associated if they were in close proximity with the
637 venous sinus, and non-sinus if they were in all other areas of the dura. For TdTM+ vessel
638 quantification in AAV-BR1-Cre injected Ai14 TdTM reporter mice, 100 vessels were randomly
639 selected from 10 different images of the cortex from 3 mice. The area of TdTM as a percent of
640 CD31 immunofluorescence was quantified.
641
642 *Cell suspension preparation from lymph nodes, spleen, and blood*
643 At the indicated timepoints, mesenteric, axillary and inguinal (non-brain draining) lymph nodes
644 were extracted from each animal and pooled, placed on a premoistened 70-μm cell strainer,
645 gently triturated, washed with 10 mL of PBS and spun at 500*g* for 7 min[24]. The cell suspension

646 was then either stained for flow cytometry analysis or processed for analysis of intracellular
647 cytokines. The spleen was removed, its epithelium was cut longitudinally, and cells were
648 isolated as described for the lymph nodes. Blood (150 μL) was drained from the submandibular
649 venous plexus into heparinized tubes, incubated with erythrocytes lysis buffer and spun at
650 500*g* for 7 min, and cells were stained for flow cytometry analysis[24].
651
652 *Isolation of intestinal lamina propria mononuclear cells*
653 Mice were euthanized by isoflurane overdose, and small intestines were removed and
654 separated as previously described[24, 30]. Peyer patches were cut out from the small intestine and
655 small intestines were completely cleaned of mesenteric fat and intestinal contents[24]. Then
656 intestines were opened longitudinally, washed of fecal contents with PBS, cut into approximately
657 1 cm pieces and placed into 20 mL of HBSS/10 mM HEPES, 8% FBS, 4 mM EDTA, 0.5 mM
658 DTT. Next intestinal pieces were washed three times in a shaking incubator set at 250 rpm and
659 at 37 °C for 20 min. After each round, intestinal pieces were vortexed for 20 s and the cell
660 suspension containing intraepithelial lymphocytes (IELs) was collected. Suspensions from the
661 three washes of IELs were combined and filtered over 0.3 g of prewashed nylon wool placed
662 into a 10-mL syringe and then over a 70-μm strainer. Intestinal pieces were washed with
663 complete PBS to remove EDTA, minced thoroughly with scissors and placed into 5 mL of
664 0.2 mg/mL of collagenase D in HBSS/10 mM HEPES with 5% of FBS. Then the intestinal pieces
665 were digested at 250 rpm and 37 °C for 20 min, followed by 20 s of vortex. The resulting cell
666 suspension contained the LPMCs, and was filtered with a 40-μm nylon cell strainer; the strainer
667 was washed with 10 mL of PBS. LPMCs cell suspensions were spun at 500*g* for 10 min at 4 °C.
668 Cell pellets were resuspended in 8 mL 44% Percoll and overlaid on 5 mL of 67% Percoll.
669 Gradients were centrifuged at 500*g* for 20 min at 4 °C (without brake) and cells at the interface
670 were collected and washed with 10 mL of PBS. Cells were then spun at 500*g* for 10 min at 4 °C
671 and cells were stained for flow cytometry analysis.

672

673 *Flow cytometry and fluorescence activated cell sorting*

674 For surface marker analysis, 1 × 10^6 cells approximately were resuspended in 50 µL of FACS
675 buffer. Cells were blocked with anti-CD16/CD32 for 10 min at 4 °C and then stained with the
676 appropriate antibodies for 15 minutes at 4 °C. Antibodies and concentrations used are listed in
677 Supplementary table 4. Cells were washed with FACS buffer, resuspended in 200 µL of FACS
678 buffer and acquired NovoSampler Q (NovoCyte Quanteon), and absolute cell numbers and
679 frequencies were recorded. Samples were analyzed with FlowJo (Vers.10, Tree Star) by an
680 investigator blinded to the treatment groups (Suppl Figs 3, 4, and 9). Appropriate isotype
681 controls, "fluorescence minus one" staining, and staining of negative populations were used to
682 establish sorting parameters. Endothelial cells were identified as $CD45^-Ly6C^+$, microglia were
683 identified as $CD45^{int}CD11b^{+}$[33]. Brain macrophages were identified as $CD45^{hi}CD11b^{+}CD36^{+}$[26, 41,
684 91-93]. We could not use the canonical BAM marker CD206 because this approach requires cell
685 permeabilization for intracellular antibody access and cannot be used in conjunction with live
686 cells assays, such as those for measuring ROS production. Therefore, we used CD36 as a
687 marker of BAM, as shown by single-cell RNA sequencing data[37]. To validate this approach, we
688 quantified the overlap of CD206 and CD36 expression within the CD45 and CD11b population.
689 We found that close to 90% of CD206 cells express CD36 (Suppl Fig 8) attesting to the validity
690 of this approach. For fluorescence activated cell sorting, endothelial and microglia cells (Suppl
691 Fig 7) were sorted on a FACSAria II (BD Biosciences) or CytoFlex SRT (Beckman) and
692 collected in sample buffer for genomic DNA qRT-PCR.

693

694 *Cerebral endothelial knockdown of IL17-RA*

695 Seven-ten week-old C57BL/6J, B6.Cg-*Gt(ROSA)26Sor*$^{tm14(CAG\text{-}tdTomato)Hze}$/J (Ai14 TdTomato
696 reporter, Stock #007909), and IL-17RA$^{flox/flox}$ mice[34] mice were administered 1.8x10^{11} VG in
697 100µL sterile PBS of AAV-BR1-iCre[32, 33] (AAV-NRGTEWD-CAG-iCre). In Ai14 TdTomato mice,

698 virus transduction was assessed by immunofluorescence (described above) and analyzed as
699 TdTomato colocalization with the endothelial CD31 marker (100 vessels per mouse; n=3 mice).
700 In IL-17RA$^{flox/flox}$ mice, DOCA pellets were implanted three weeks after AAV-BR1-iCre
701 administration.
702
703 *Nitric oxide measurement in pial microvessels*
704 Pial microvessels were removed under a dissecting microscope[94] and incubated with DAF-FM
705 (25 μM; Molecular Probes) in l-ACSF (124 mM NaCl, 26 mM $NaHCO_3$, 5 mM KCl, 1 mM
706 NaH_2PO_4, 2 mM $CaCl_2$, 2 mM $MgSO_4$, 20 mM glucose, 4.5 mM lactic acid, oxygenated with 95%
707 O_2 and 5% CO2, pH=7.4) at room temperature for 45 min[24, 94]. Time-resolved fluorescence was
708 measured every 60 s with an exposure time of 150 ms using image analysis software (IPLab,
709 Scanalytics Inc). After a stable fluorescence baseline was achieved, microvessels were
710 superfused with ACh (100 μM) for 15 min. DAF-FM fluorescence intensity is expressed as
711 RFU/μm^2, where RFU is the relative fluorescence unit, and μm^2 is unit of the area in which RFU
712 was measured.
713
714 *Western blotting*
715 Cerebral blood vessels and brain microvascular endothelial cells samples were lysed in RIPA
716 buffer (50 mM Tris-HCl pH 8.0, 150 mM NaCl, 0.5% deoxycholic acid, 0.1% SDS, 1 mM EDTA
717 pH 8.0, 1% IGEPAL CA-630) and equal volumes were mixed with SDS sample buffer, boiled,
718 and analyzed on 4–12% SDS polyacrylamide gels. Proteins were transferred to PVDF
719 membranes (Millipore), blocked with 5% milk in TBS/0.1% Tween-20 (TBST) and incubated with
720 anti-phospho-eNOS (Thr^{495}) and anti-eNOS (Suppl Table 3; 1:1,000, Cell Signaling cat. #9574
721 and 9572, respectively). Membranes were washed in TBST, incubated with goat anti-rabbit
722 secondary antibodies conjugated to horseradish peroxidase (1:5,000; Jackson
723 ImmunoResearch peroxidase affinity-purified whole IgG antibodies), and protein bands were

724 visualized with Clarity Western ECL Substrate (Bio-Rad) on a Bio-Rad ChemiDoc MP Imaging
725 System. Raw images are provided in Suppl Fig 17-22.
726
727 *In vivo treatments*
728 To deplete cerebral CD206^{+} brain macrophages, clodronate- or PBS-loaded liposomes were
729 prepared as previously described[23, 33]. Under isoflurane anesthesia, 10 µl of clodronate-
730 liposomes (7 mg/ml) and PBS-liposomes (vehicle) were injected (rate: 500 nl/min, approaching
731 CSF clearance rates 300-400 nl/min[95]) into the cerebral ventricles (i.c.v.) with a Hamilton
732 syringe through a burr hole drilled on the right parietal bone (coordinates: 0.5 mm posterior to
733 bregma 1.0 mm lateral from midline, 2.3 mm below the brain surface) on the same day as
734 DOCA pellet implantation. Assessments were made 21 days after the injection, allowing ample
735 time for any potential perturbations in CSF homeostasis to subside. Attesting to the lack of
736 untoward effects of the injection we did not observe any alterations in cerebrovascular
737 regulation (functional hyperemia, endothelial vasoactivity, smooth muscle vasomotor function),
738 BBB permeability, or cognition in mice injected with the same volume of control PBS-liposomes.
739 FTY720 (1 mg/kg; Cayman Chemical)[24] was injected i.p. three times every 3 d after the first
740 week of DOCA-salt. Control and DOCA-salt mice were equipped with an intracerebroventricular
741 (i.c.v.) cannula attached to a osmotic mini-pump (ALZET brain infusion kit 3 #0008851, pump
742 #1004) for delivery of anti-TCR$\gamma\delta$ antibody (UC7-13D5, BioXCell 0.1μg/hr) or isotype control
743 (polyclonal Armenian hamster IgG, BioXCell) on day 7 of DOCA salt. i.c.v. delivery of losartan
744 (5μg/hour) or saline was started on the same day as DOCA pellet implantation.
745
746 *Isolation of brain and dural leukocytes*
747 Isolation of brain leukocytes was performed as described[33]. Mice were anesthetized with
748 pentobarbital (100 mg/kg, i.p.) and transcardially perfused with heparinized PBS. Brain cell

749 isolation was performed by enzymatic digestion with Liberase DH (Roche Diagnostics) and
750 Dispase (Worthington). Brain hemispheres were separated from the cerebellum and olfactory
751 bulb and gently triturated in HEPES-HBSS buffer containing the following: 138mM NaCl, 5mM
752 KCl, 0.4mM Na_2HPO_4, 0.4mM KH_2PO_4, 5mM d-glucose, and 10mM HEPES using a Gentle
753 MACS dissociator (Miltenyi Biotec) following the manufacturer's instructions. The dura was
754 stripped from the skull[90] using a dissection microscope. The suspension was digested with 125
755 µg/ml Liberase, 0.8U/ml dispase, and 50 U/ml DNase I at 37°C for 45 min (brain) or 15 min
756 (dura) in an orbital shaker at 100 rpm. Brain cells isolated were washed and subjected to 30%
757 Percoll (GE Healthcare) density gradient centrifugation at 500*g* for 15 min. Dura were placed on
758 the surface of a premoistened 70-µm cell strainer. Tissue was gently homogenized with the end
759 of a 1-mL syringe plunger, washed with 20 mL 2% FBS in PBS and centrifuged at 500*g* for
760 7 min.
761
762 *ROS assessment by flow cytometry*
763 Following isolation of brain leukocytes, cells were incubated with dihydroethidium (DHE, 2.5µM)
764 or dichlorodihydrofluorescein diacetate (DCF, 2µM) in stimulation buffer (RPMI-1640, 10% (v/v)
765 heat inactivated FBS, 100 units/mL penicillin, 100 µg/mL streptomycin) for 30 minutes at 37°
766 and 5% CO_2. Some cells were pooled and separated for stimulation experiments, and were
767 incubated with PBS, murine recombinant IL-17 (10ng/mL, Preprotech), or Ang II (300nM,
768 Sigma) for 30 minutes prior to addition of DHE (as above). Cells were washed with FACS buffer
769 (1X PBS, 2% FBS, 0.05% NaN_3) and centrifuged at 500*g* for 7 min.
770
771 *Bone marrow transplant*
772 As previously described[23, 33], whole-body irradiation was performed on 6-week-old C57BL/6
773 male mice with a lethal dose of 9.5 Gy of γ radiation using a ^{137}Cs source (Nordion Gammacell

774 40 Exactor). Eighteen hours later, BM cells (2×10^6, i.v.) isolated from donor IL-17RA knockout
775 mice or B6.129S-*Cybb*^{tm1Din}/J mice (*Nox2*$^{-/-}$, JAX stock# 002365) were transplanted in irradiated
776 mice. Mice with transplanted BM cells were housed in cages with Sulfatrim diet for the first 2
777 weeks.
778
779 *qRT-PCR*
780 Procedures for RT-PCR were identical to those previously described[23, 24, 33]. Briefly, samples
781 were collected in TRIzol (Invitrogen Life Technologies) and RNA was extracted according to the
782 manufacturer's instructions. RNA samples were treated with Rnase-free DnaseI (Roche) to
783 remove DNA contamination. cDNA was produced from mRNA samples using the iScript
784 Reverse Transcription Supermix (Bio-Rad). Quantitative determination of gene expression was
785 performed on a Quantstudio 5 (Applied Biosystems). Hypoxanthine-guanine
786 phosphoribosyltransferase (HPRT) was used to normalize gene expression. qRT-PCR was
787 conducted with cDNA in duplicate 10-μL reactions on a 384-well plate using the Maxim a SYBR
788 Green/ROX qPCR Master Mix (2×) (Thermo Scientific). The reactions were incubated at 50°C
789 for 2 min and then at 95°C for 10 min. A polymerase chain reaction cycling protocol consisting
790 of 15 s at 95°C and 1 min at 60°C for 45 cycles was used for quantification. Relative expression
791 levels were calculated according to Livak and Schmittgen, and values were normalized to
792 respective normal control samples. Reference primer sequences are described in Suppl table 4.
793 For assessment of *Il17ra* knockdown *in vivo*, genomic DNA was extracted from sorted
794 endothelial and microglia cells. Cre recombination specifically targets exons 4-7 of the *Il17ra*
795 gene in IL17-RA$^{flox/flox}$ mice, thus we normalized *Il17ra* exon 5 expression to the non-targeted
796 *Il17ra* exon 3. Primer sequences as described in Suppl table 4.
797
798 *RNAscope*

799 Tissue was treated according to manufacture's instructions for the RNAScope Multiplex
800 Fluorescent v2 Assay. Following 2% PFA perfusion, brain tissue was left in 2% PFA overnight.
801 The tissue then went through a sequential sucrose gradient (10%, 20%, 30%) before freezing
802 and storing at -80C. Tissue was cut at 10um on a cryostat, mounted on charged slides, and
803 stored at -80C until use. Slides were left to warm up for 2 hours at -20C then baked at 60C for
804 30+ min. Slides were washed with 1x PBS for 5 min then treated with RNAScope Hydrogen
805 Peroxide for 10 min. Slides were washed with nuclease-free water and pretreated with target
806 retrieval buffer in a slide envelope placed in 100C boiling water for 5 min. Slides were then
807 washed with distilled water, dipped in 100% EtOH, and a barrier was established around the
808 tissue using a hydrophobic marker. Slides were then allowed to air dry overnight. Slides were
809 treated with Protease IV for 15 min at 40C, followed by a probe incubation for 2 hours at 40C.
810 The probes (purchased from ACD) used were Mm-Mrc1 (Cat # 437511) and Mm-Il17ra-O1-C2
811 (Cat # 566131-C2). A 3-plex positive control probe and 3-plex negative control were run
812 concurrently. After probe incubation, slides underwent three amplification steps (RNAScope
813 Multiplex Fluorescent Detection Reagents v2, ACD, Cat # 323110) followed by the development
814 of horseradish peroxidase (HRP) signal fluorescence with TSA-based fluorophores. HRP
815 blockers were used after every fluorophore incubation. After each step, slides were washed
816 twice with wash buffer. Slides were then treated with RNAScope DAPI for 30 seconds then
817 cover-slipped in Fluorosave Reagent (Sigma, Cat # 345789) and left to dry for 20 min. Slides
818 were then stored at 4C until imaging.
819
820 *IL-17A ELISpot Assay*
821 Dura leukocytes were isolated as described above, and incubated in ELISpot plate for 4 hours
822 in stimulation buffer (RPMI-1640, 10% (v/v) heat inactivated FBS, 100 units/mL penicillin, 100
823 μg/mL streptomycin, 100 ng/mL phorbol 12-myristate 13-acetate (PMA), 1 μg/mL of ionomycin)
824 in a 37C humidified incubator with 5% CO2. Mouse IL-17A ELISpotPLUS kit ALP (MABTECH,

825 Cat# 3521-4APW-2) was performed following manufacturer's instructions. Wells were
826 developed with BCIP/NBT-plus for 15 minutes, and color development was stopped by washing
827 with diH2O. Images were obtained using a digital camera (T TAKMLY, MX200-B) and analyzed
828 using ImageJ software.
829
830 *CSF Collection*
831 Mice were anesthetized with isoflurane (3% induction, 1.5% maintenance), and placed on a
832 stereotaxic frame with the head slightly tilted forward. A small incision was made over the back
833 of the neck, and muscle tissue moved to expose the dura over the cisterna magna. The area
834 was cleaned with a cotton bud. Heparinized glass capillaries were prepared using a
835 micropipette puller, attached to a thin tube and syringe connected through a three-way valve,
836 and mounted on a micromanipulator[96]. Under a dissecting microscope, the glass capillary was
837 aligned to the cisterna magna, avoiding blood vessels in the area, and tapped through the dura
838 to collect CSF for a maximum of 10 minutes. On average, 15-18μl was obtained per mouse.
839 Equal volumes of CSF from two animals were pooled to maximize loading sample volume of
840 25μl for IL-17 quantification (Mesoscale).
841
842 *Ang II assay*
843 Mice were euthanized, and blood was collected by cardiac puncture in a prechilled tube
844 containing a mix of protease inhibitors. Plasma was collected and transferred to a prechilled
845 tube and stored frozen at –80°C. Brains were collected and immediately frozen on dry ice. Ang
846 II concentration was determined using a radioimmunoassay by the Hypertension Core
847 Laboratory of the Wake Forest University School of Medicine (Winston-Salem, North Carolina,
848 USA)[97].
849

850 *Statistical analysis*

851 Sample size was determined according to standard power analysis (80% power and α=0.05)
852 based on standardized effect sizes calculated from published studies[23, 24, 30, 88, 98]. Animals were
853 randomly assigned to treatment and control groups, and analysis was performed in a blinded
854 fashion. After testing for normality (Bartlett's test), intergroup differences were analyzed by
855 unpaired two-tailed t-test for single comparison, or by 1-way ANOVA or 2-way ANOVA with
856 Tukey's or Bonferroni's multiple comparison test, as appropriate and indicated in the figure
857 legends. If non-parametric testing was indicated, intergroup differences were analyzed by
858 Mann-Whitney test or Kruskal-Wallis test with Dunn's correction, as appropriate and indicated in
859 the figure legends. Statistical tests through the manuscript were performed using Prism 7
860 (GraphPad). All data are presented as mean ± SEM.

861

862 ACKNOWLEDGEMENTS

863 This work was supported by grants R37-NS089323 (CI), R01-NS095441(CI) and K22-
864 NS123507 (MMS), as well as the Leon Levy Fellowship in Neuroscience (MMS). The support
865 from the Feil Family Foundation is gratefully acknowledged. The authors declare no competing
866 financial interests. Figure schematics were made on Biorender.

867

868 REFERENCES

869 1. Levine DA, Springer MV, Brodtmann A. Blood pressure and vascular cognitive
870 impairment. *Stroke*. 2022;53:1104-1113
871 2. Muntner P, Miles MA, Jaeger BC, Hannon L, 3rd, Hardy ST, Ostchega Y, et al. Blood
872 pressure control among us adults, 2009 to 2012 through 2017 to 2020. *Hypertension*.
873 2022:101161hypertensionaha12219222
874 3. Carey RM, Sakhuja S, Calhoun DA, Whelton PK, Muntner P. Prevalence of apparent
875 treatment-resistant hypertension in the united states. *Hypertension*. 2019;73:424-431
876 4. Williamson JD, Pajewski NM, Auchus AP, Bryan RN, Chelune G, Cheung AK, et al.
877 Effect of intensive vs standard blood pressure control on probable dementia: A
878 randomized clinical trial. *Jama*. 2019;321:553-561
879 5. Webb AJS, Werring DJ. New insights into cerebrovascular pathophysiology and
880 hypertension. *Stroke*. 2022;53:1054-1064

6. Iadecola C, Gottesman RF. Neurovascular and cognitive dysfunction in hypertension: Epidemiology, pathobiology and treatment. *Circ Res*. 2019;124:1025-1044
7. Oh YS, Appel LJ, Galis ZS, Hafler DA, He J, Hernandez AL, et al. National heart, lung, and blood institute working group report on salt in human health and sickness: Building on the current scientific evidence. *Hypertension*. 2016;68:281-288
8. Elijovich F, Weinberger MH, Anderson CA, Appel LJ, Bursztyn M, Cook NR, et al. Salt sensitivity of blood pressure: A scientific statement from the american heart association. *Hypertension*. 2016;68:e7-e46
9. Grobe JL, Buehrer BA, Hilzendeger AM, Liu X, Davis DR, Xu D, et al. Angiotensinergic signaling in the brain mediates metabolic effects of deoxycorticosterone (doca)-salt in c57 mice. *Hypertension*. 2011;57:600-607
10. Basting T, Lazartigues E. Doca-salt hypertension: An update. *Curr Hypertens Rep*. 2017;19:32
11. Meade TW, Imeson JD, Gordon D, Peart WS. The epidemiology of plasma renin. *Clin Sci (Lond)*. 1983;64:273-280
12. Alderman MH, Madhavan S, Ooi WL, Cohen H, Sealey JE, Laragh JH. Association of the renin-sodium profile with the risk of myocardial infarction in patients with hypertension. *N Engl J Med*. 1991;324:1098-1104
13. Madhur MS, Lob HE, McCann LA, Iwakura Y, Blinder Y, Guzik TJ, et al. Interleukin 17 promotes angiotensin ii-induced hypertension and vascular dysfunction. *Hypertension*. 2010;55:500-507
14. Yao W, Sun Y, Wang X, Niu K. Elevated serum level of interleukin 17 in a population with prehypertension. *J Clin Hypertens (Greenwich)*. 2015;17:770-774
15. Simundic T, Jelakovic B, Dzumhur A, Turk T, Sahinovic I, Dobrosevic B, et al. Interleukin 17a and toll-like receptor 4 in patients with arterial hypertension. *Kidney Blood Press Res*. 2017;42:99-108
16. Kleinewietfeld M, Manzel A, Titze J, Kvakan H, Yosef N, Linker RA, et al. Sodium chloride drives autoimmune disease by the induction of pathogenic th17 cells. *Nature*. 2013;496:518-522
17. Wilck N, Matus MG, Kearney SM, Olesen SW, Forslund K, Bartolomaeus H, et al. Salt-responsive gut commensal modulates th17 axis and disease. *Nature*. 2017;551:585-589
18. Wu C, Yosef N, Thalhamer T, Zhu C, Xiao S, Kishi Y, et al. Induction of pathogenic th17 cells by inducible salt-sensing kinase sgk1. *Nature*. 2013;496:513-517
19. Faraco G, Park L, Anrather J, Iadecola C. Brain perivascular macrophages: Characterization and functional roles in health and disease. *J Mol Med (Berl)*. 2017;95:1143-1152
20. Kierdorf K, Masuda T, Jordao MJC, Prinz M. Macrophages at cns interfaces: Ontogeny and function in health and disease. *Nat Rev Neurosci*. 2019;20:547-562
21. Faraco G, Park L, Zhou P, Luo W, Paul SM, Anrather J, et al. Hypertension enhances abeta-induced neurovascular dysfunction, promotes beta-secretase activity, and leads to amyloidogenic processing of app. *J Cereb Blood Flow Metab*. 2016;36:241-252
22. Kopp C, Linz P, Dahlmann A, Hammon M, Jantsch J, Müller DN, et al. 23na magnetic resonance imaging-determined tissue sodium in healthy subjects and hypertensive patients. *Hypertension*. 2013;61:635-640
23. Faraco G, Sugiyama Y, Lane D, Garcia-Bonilla L, Chang H, Santisteban MM, et al. Perivascular macrophages mediate the neurovascular and cognitive dysfunction associated with hypertension. *J Clin Invest*. 2016;126:4674-4689
24. Faraco G, Brea D, Garcia-Bonilla L, Wang G, Racchumi G, Chang H, et al. Dietary salt promotes neurovascular and cognitive dysfunction through a gut-initiated th17 response. *Nat Neurosci*. 2018;21:240-249

25. Toda N, Ayajiki K, Okamura T. Cerebral blood flow regulation by nitric oxide: Recent advances. *Pharmacol Rev*. 2009;61:62-97
26. Iadecola C, Smith EE, Anrather J, Gu C, Mishra A, Misra S, et al. The neurovasculome: Key roles in brain health and cognitive impairment: A scientific statement from the american heart association/american stroke association. *Stroke*. 2023
27. Itani HA, McMaster WG, Jr., Saleh MA, Nazarewicz RR, Mikolajczyk TP, Kaszuba AM, et al. Activation of human t cells in hypertension: Studies of humanized mice and hypertensive humans. *Hypertension*. 2016;68:123-132
28. Kim S, Goel R, Kumar A, Qi Y, Lobaton G, Hosaka K, et al. Imbalance of gut microbiome and intestinal epithelial barrier dysfunction in patients with high blood pressure. *Clin Sci (Lond)*. 2018;132:701-718
29. Esplugues E, Huber S, Gagliani N, Hauser AE, Town T, Wan YY, et al. Control of th17 cells occurs in the small intestine. *Nature*. 2011;475:514-518
30. Benakis C, Brea D, Caballero S, Faraco G, Moore J, Murphy M, et al. Commensal microbiota affects ischemic stroke outcome by regulating intestinal gammadelta t cells. *Nat Med*. 2016;22:516-523
31. Maeda Y, Seki N, Kataoka H, Takemoto K, Utsumi H, Fukunari A, et al. Il-17-producing vγ4+ γδ t cells require sphingosine 1-phosphate receptor 1 for their egress from the lymph nodes under homeostatic and inflammatory conditions. *J Immunol*. 2015;195:1408-1416
32. Korbelin J, Dogbevia G, Michelfelder S, Ridder DA, Hunger A, Wenzel J, et al. A brain microvasculature endothelial cell-specific viral vector with the potential to treat neurovascular and neurological diseases. *EMBO Mol Med*. 2016;8:609-625
33. Santisteban MM, Ahn SJ, Lane D, Faraco G, Garcia-Bonilla L, Racchumi G, et al. Endothelium-macrophage crosstalk mediates blood-brain barrier dysfunction in hypertension. *Hypertension*. 2020;76:795-807
34. El Malki K, Karbach SH, Huppert J, Zayoud M, Reissig S, Schuler R, et al. An alternative pathway of imiquimod-induced psoriasis-like skin inflammation in the absence of interleukin-17 receptor a signaling. *J Invest Dermatol*. 2013;133:441-451
35. Schaeffer S, Iadecola C. Revisiting the neurovascular unit. *Nat Neurosci*. 2021;24:1198-1209
36. Nikolakopoulou AM, Wang Y, Ma Q, Sagare AP, Montagne A, Huuskonen MT, et al. Endothelial lrp1 protects against neurodegeneration by blocking cyclophilin a. *J Exp Med*. 2021;218
37. Van Hove H, Martens L, Scheyltjens I, De Vlaminck K, Pombo Antunes AR, De Prijck S, et al. A single-cell atlas of mouse brain macrophages reveals unique transcriptional identities shaped by ontogeny and tissue environment. *Nat Neurosci*. 2019;22:1021-1035
38. Park L, Uekawa K, Garcia-Bonilla L, Koizumi K, Murphy M, Pistik R, et al. Brain perivascular macrophages initiate the neurovascular dysfunction of alzheimer abeta peptides. *Circ Res*. 2017;121:258-269
39. Sayd A, Vargas-Caraveo A, Perea-Romero I, Robledo-Montaña J, Caso JR, Madrigal JLM, et al. Depletion of brain perivascular macrophages regulates acute restraint stress-induced neuroinflammation and oxidative/nitrosative stress in rat frontal cortex. *Eur Neuropsychopharmacol*. 2020;34:50-64
40. Mendiola AS, Ryu JK, Bardehle S, Meyer-Franke A, Ang KK, Wilson C, et al. Transcriptional profiling and therapeutic targeting of oxidative stress in neuroinflammation. *Nat Immunol*. 2020;21:513-524
41. Ivan DC, Walthert S, Berve K, Steudler J, Locatelli G. Dwellers and trespassers: Mononuclear phagocytes at the borders of the central nervous system. *Front Immunol*. 2020;11:609921

42. Garcia-Bonilla L, Sciortino R, Shahanoor Z, Racchumi G, Janakiraman M, Montaner J, et al. Role of microglial and endothelial cd36 in post-ischemic inflammasome activation and interleukin-1β-induced endothelial activation. *Brain Behav Immun*. 2021;95:489-501
43. Hohsfield LA, Najafi AR, Ghorbanian Y, Soni N, Hingco EE, Kim SJ, et al. Effects of long-term and brain-wide colonization of peripheral bone marrow-derived myeloid cells in the cns. *J Neuroinflammation*. 2020;17:279
44. Chinnery HR, Ruitenberg MJ, McMenamin PG. Novel characterization of monocyte-derived cell populations in the meninges and choroid plexus and their rates of replenishment in bone marrow chimeric mice. *J Neuropathol Exp Neurol*. 2010;69:896-909
45. Pietrowski E, Bender B, Huppert J, White R, Luhmann HJ, Kuhlmann CR. Pro-inflammatory effects of interleukin-17a on vascular smooth muscle cells involve nad(p)h-oxidase derived reactive oxygen species. *J Vasc Res*. 2011;48:52-58
46. Louveau A, Herz J, Alme MN, Salvador AF, Dong MQ, Viar KE, et al. Cns lymphatic drainage and neuroinflammation are regulated by meningeal lymphatic vasculature. *Nat Neurosci*. 2018;21:1380-1391
47. Rua R, McGavern DB. Advances in meningeal immunity. *Trends Mol Med*. 2018;24:542-559
48. Alves de Lima K, Rustenhoven J, Da Mesquita S, Wall M, Salvador AF, Smirnov I, et al. Meningeal γδ t cells regulate anxiety-like behavior via il-17a signaling in neurons. *Nat Immunol*. 2020
49. Ribeiro M, Brigas HC, Temido-Ferreira M, Pousinha PA, Regen T, Santa C, et al. Meningeal γδ t cell-derived il-17 controls synaptic plasticity and short-term memory. *Sci Immunol*. 2019;4
50. Rustenhoven J, Drieu A, Mamuladze T, de Lima KA, Dykstra T, Wall M, et al. Functional characterization of the dural sinuses as a neuroimmune interface. *Cell*. 2021;184:1000-1016.e1027
51. Ranieri E, Netti GS, Gigante M. Ctl elispot assay and t cell detection. *Methods Mol Biol*. 2021;2325:65-77
52. Jones HE, Abrams KA, Siegenthaler JA. Techniques for visualizing fibroblast-vessel interactions in the developing and adult cns. *Neurophotonics*. 2022;9:021911
53. Derk J, Como CN, Jones HE, Joyce LR, Kim S, Spencer BL, et al. Formation and function of the meningeal arachnoid barrier around the developing mouse brain. *Dev Cell*. 2023
54. Zhang Y, Bailey JT, Xu E, Singh K, Lavaert M, Link VM, et al. Mucosal-associated invariant t cells restrict reactive oxidative damage and preserve meningeal barrier integrity and cognitive function. *Nat Immunol*. 2022;23:1714-1725
55. Prinz I, Silva-Santos B, Pennington DJ. Functional development of γδ t cells. *Eur J Immunol*. 2013;43:1988-1994
56. Gray EE, Ramírez-Valle F, Xu Y, Wu S, Wu Z, Karjalainen KE, et al. Deficiency in il-17-committed vγ4(+) γδ t cells in a spontaneous sox13-mutant cd45.1(+) congenic mouse substrain provides protection from dermatitis. *Nat Immunol*. 2013;14:584-592
57. McKenzie DR, Kara EE, Bastow CR, Tyllis TS, Fenix KA, Gregor CE, et al. Il-17-producing γδ t cells switch migratory patterns between resting and activated states. *Nat Commun*. 2017;8:15632
58. Mandala S, Hajdu R, Bergstrom J, Quackenbush E, Xie J, Milligan J, et al. Alteration of lymphocyte trafficking by sphingosine-1-phosphate receptor agonists. *Science*. 2002;296:346-349
59. Chiba K, Yanagawa Y, Masubuchi Y, Kataoka H, Kawaguchi T, Ohtsuki M, et al. Fty720, a novel immunosuppressant, induces sequestration of circulating mature lymphocytes by acceleration of lymphocyte homing in rats. *J Immunol*. 1998;160:5037-5044

1033 60. Enosawa S, Suzuki S, Kakefuda T, Li XK, Amemiya H. Induction of selective cell death
1034 targeting on mature t-lymphocytes in rats by a novel immunosuppressant, fty720.
1035 *Immunopharmacology*. 1996;34:171-179
1036 61. Krebs CF, Paust HJ, Krohn S, Koyro T, Brix SR, Riedel JH, et al. Autoimmune renal
1037 disease is exacerbated by s1p-receptor-1-dependent intestinal th17 cell migration to the
1038 kidney. *Immunity*. 2016;45:1078-1092
1039 62. De Silva TM, Modrick ML, Grobe JL, Faraci FM. Activation of the central renin-
1040 angiotensin system causes local cerebrovascular dysfunction. *Stroke*. 2021;52:2404-
1041 2413
1042 63. Lu X, Crowley SD. The immune system in hypertension: A lost shaker of salt 2021 lewis
1043 k. Dahl memorial lecture. *Hypertension*. 2022;79:1339-1347
1044 64. Guzik TJ, Hoch NE, Brown KA, McCann LA, Rahman A, Dikalov S, et al. Role of the t
1045 cell in the genesis of angiotensin ii induced hypertension and vascular dysfunction. *J*
1046 *Exp Med*. 2007;204:2449-2460
1047 65. Norlander AE, Madhur MS, Harrison DG. The immunology of hypertension. *J Exp Med*.
1048 2018;215:21-33
1049 66. Drummond GR, Vinh A, Guzik TJ, Sobey CG. Immune mechanisms of hypertension. *Nat*
1050 *Rev Immunol*. 2019;19:517-532
1051 67. Higaki A, Mahmoud AUM, Paradis P, Schiffrin EL. Role of interleukin-23/interleukin-17
1052 axis in t-cell mediated actions in hypertension. *Cardiovasc Res*. 2020;117:1274-1283
1053 68. Lerman LO, Kurtz TW, Touyz RM, Ellison DH, Chade AR, Crowley SD, et al. Animal
1054 models of hypertension: A scientific statement from the american heart association.
1055 *Hypertension*. 2019:e87-e120
1056 69. Carvalho C, Moreira PI. Oxidative stress: A major player in cerebrovascular alterations
1057 associated to neurodegenerative events. *Front Physiol*. 2018;9:806
1058 70. Gorelick PB, Scuteri A, Black SE, Decarli C, Greenberg SM, Iadecola C, et al. Vascular
1059 contributions to cognitive impairment and dementia: A statement for healthcare
1060 professionals from the american heart association/american stroke association. *Stroke*.
1061 2011;42:2672-2713
1062 71. Cortes-Canteli M, Iadecola C. Alzheimer's disease and vascular aging: Jacc focus
1063 seminar. *J Am Coll Cardiol*. 2020;75:942-951
1064 72. Brigas HC, Ribeiro M, Coelho JE, Gomes R, Gomez-Murcia V, Carvalho K, et al. Il-17
1065 triggers the onset of cognitive and synaptic deficits in early stages of alzheimer's
1066 disease. *Cell Rep*. 2021;36:109574
1067 73. Salvador AF, de Lima KA, Kipnis J. Neuromodulation by the immune system: A focus on
1068 cytokines. *Nat Rev Immunol*. 2021;21:526-541
1069 74. Rouch L, Cestac P, Hanon O, Cool C, Helmer C, Bouhanick B, et al. Antihypertensive
1070 drugs, prevention of cognitive decline and dementia: A systematic review of
1071 observational studies, randomized controlled trials and meta-analyses, with discussion
1072 of potential mechanisms. *CNS Drugs*. 2015;29:113-130
1073 75. Ding J, Davis-Plourde KL, Sedaghat S, Tully PJ, Wang W, Phillips C, et al.
1074 Antihypertensive medications and risk for incident dementia and alzheimer's disease: A
1075 meta-analysis of individual participant data from prospective cohort studies. *Lancet*
1076 *Neurol*. 2020;19:61-70
1077 76. James PA, Oparil S, Carter BL, Cushman WC, Dennison-Himmelfarb C, Handler J, et al.
1078 2014 evidence-based guideline for the management of high blood pressure in adults:
1079 Report from the panel members appointed to the eighth joint national committee (jnc 8).
1080 *Jama*. 2014;311:507-520
1081 77. Harrison DG, Coffman TM, Wilcox CS. Pathophysiology of hypertension: The mosaic
1082 theory and beyond. *Circ Res*. 2021;128:847-863

78. Ridker PM, Everett BM, Thuren T, MacFadyen JG, Chang WH, Ballantyne C, et al. Antiinflammatory therapy with canakinumab for atherosclerotic disease. *N Engl J Med*. 2017;377:1119-1131
79. Ma T, Wang F, Xu S, Huang JH. Meningeal immunity: Structure, function and a potential therapeutic target of neurodegenerative diseases. *Brain Behav Immun*. 2021;93:264-276
80. Hayashi S, Lewis P, Pevny L, McMahon AP. Efficient gene modulation in mouse epiblast using a sox2cre transgenic mouse strain. *Mech Dev*. 2002;119 Suppl 1:S97-s101
81. Belanger KM, Crislip GR, Gillis EE, Abdelbary M, Musall JB, Mohamed R, et al. Greater t regulatory cells in females attenuate doca-salt-induced increases in blood pressure versus males. *Hypertension*. 2020;75:1615-1623
82. Korvela M, Lind AL, Wetterhall M, Gordh T, Andersson M, Pettersson J. Quantification of 10 elements in human cerebrospinal fluid from chronic pain patients with and without spinal cord stimulation. *J Trace Elem Med Biol*. 2016;37:1-7
83. Bischoff K, Lamm C, Erb HN, Hillebrandt JR. The effects of formalin fixation and tissue embedding of bovine liver on copper, iron, and zinc analysis. *J Vet Diagn Invest*. 2008;20:220-224
84. Capone C, Faraco G, Park L, Cao X, Davisson RL, Iadecola C. The cerebrovascular dysfunction induced by slow pressor doses of angiotensin ii precedes the development of hypertension. *Am J Physiol Heart Circ Physiol*. 2011;300:H397-407
85. Kazama K, Wang G, Frys K, Anrather J, Iadecola C. Angiotensin ii attenuates functional hyperemia in the mouse somatosensory cortex. *Am J Physiol Heart Circ Physiol*. 2003;285:H1890-1899
86. Kober F, Iltis I, Izquierdo M, Desrois M, Ibarrola D, Cozzone PJ, et al. High-resolution myocardial perfusion mapping in small animals in vivo by spin-labeling gradient-echo imaging. *Magn Reson Med*. 2004;51:62-67
87. Deacon RM. Assessing nest building in mice. *Nat Protoc*. 2006;1:1117-1119
88. Faraco G, Hochrainer K, Segarra SG, Schaeffer S, Santisteban MM, Menon A, et al. Dietary salt promotes cognitive impairment through tau phosphorylation. *Nature*. 2019;574:686-690
89. Brea D, Poon C, Benakis C, Lubitz G, Murphy M, Iadecola C, et al. Stroke affects intestinal immune cell trafficking to the central nervous system. *Brain Behav Immun*. 2021;96:295-302
90. Louveau A, Filiano A, Kipnis J. Meningeal whole mount preparation and characterization of neural cells by flow cytometry. *Curr Protoc Immunol*. 2018;121
91. Goldmann T, Wieghofer P, Jordao MJ, Prutek F, Hagemeyer N, Frenzel K, et al. Origin, fate and dynamics of macrophages at central nervous system interfaces. *Nat Immunol*. 2016;17:797-805
92. Borst K, Prinz M. Deciphering the heterogeneity of myeloid cells during neuroinflammation in the single-cell era. *Brain Pathol*. 2020;30:1192-1207
93. Mendes NF, Velloso LA. Perivascular macrophages in high-fat diet-induced hypothalamic inflammation. *J Neuroinflammation*. 2022;19:136
94. Park L, Wang G, Zhou P, Zhou J, Pitstick R, Previti ML, et al. Scavenger receptor cd36 is essential for the cerebrovascular oxidative stress and neurovascular dysfunction induced by amyloid-beta. *Proc Natl Acad Sci U S A*. 2011;108:5063-5068
95. Rudick RA, Zirretta DK, Herndon RM. Clearance of albumin from mouse subarachnoid space: A measure of csf bulk flow. *J Neurosci Methods*. 1982;6:253-259
96. Lim NK, Moestrup V, Zhang X, Wang WA, Møller A, Huang FD. An improved method for collection of cerebrospinal fluid from anesthetized mice. *J Vis Exp*. 2018
97. Nakamoto H, Ferrario CM, Fuller SB, Robaczewski DL, Winicov E, Dean RH. Angiotensin-(1-7) and nitric oxide interaction in renovascular hypertension. *Hypertension*. 1995;25:796-802

1134 98. Park L, Hochrainer K, Hattori Y, Ahn SJ, Anfray A, Wang G, et al. Tau induces psd95-
1135 neuronal nos uncoupling and neurovascular dysfunction independent of
1136 neurodegeneration. *Nat Neurosci*. 2020;23:1079-1089
1137

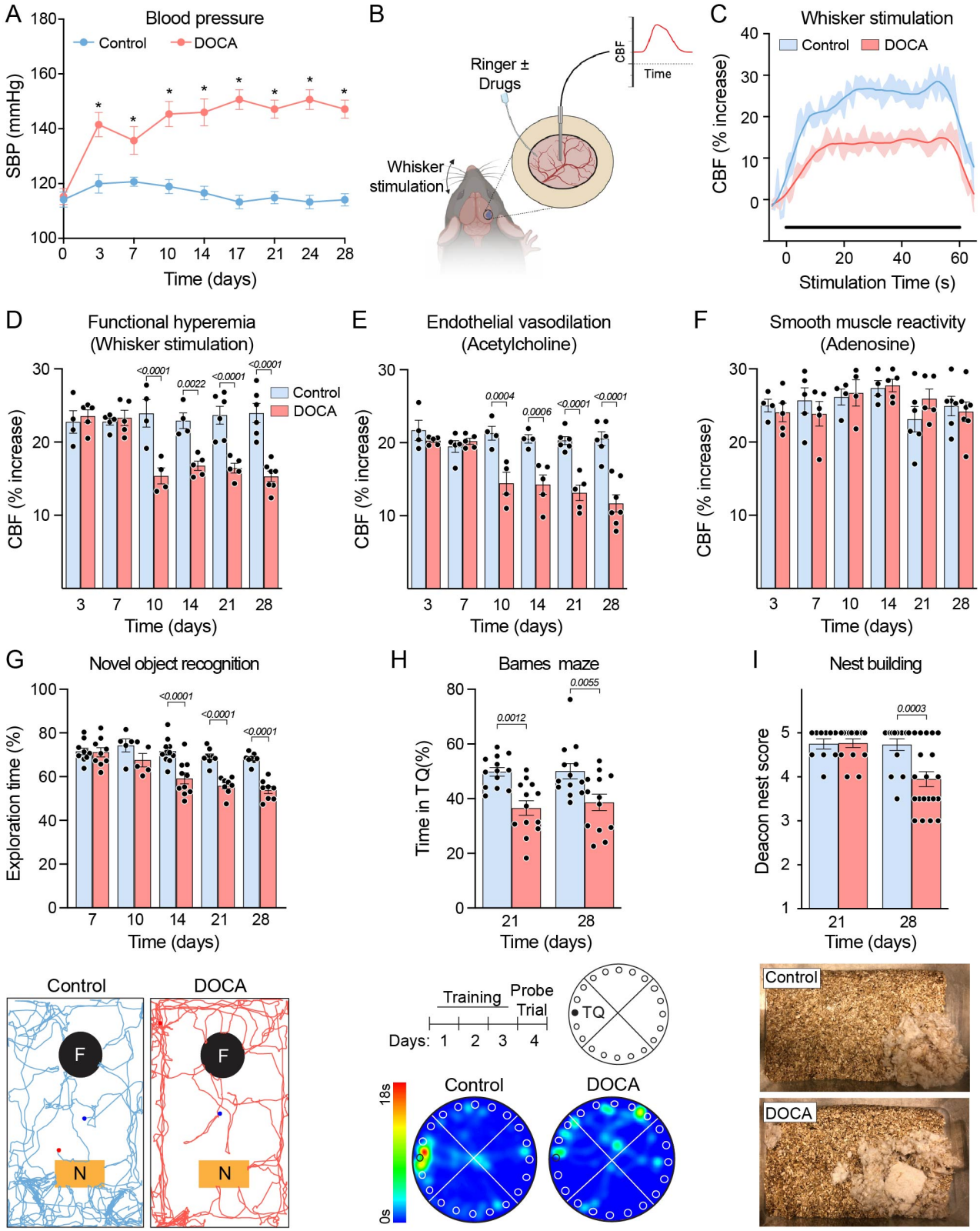

Figure 1. DOCA-salt hypertension induces neurovascular and cognitive impairment. (A) Systolic blood pressure (SBP), assessed by tail cuff plethysmography, is elevated in DOCA-salt hypertension over 28 days of treatment (HTN: p<0.0001, time: p<0.0001, interaction: p<0.0001; n=15). **(B)** Schematic of methods used to assess neurovascular function. **(C-D)** DOCA attenuates the increase in cerebral blood flow (CBF) induced by 60s stimulation of the facial whiskers (functional hyperemia),

beginning at 10 days of DOCA (HTN: $p<0.0001$, time: $p=0.001$, interaction: $p<0.0001$; n=4-7). **(E)** Endothelial vasodilation was attenuated by DOCA beginning at 10 days (HTN: $p<0.0001$, time: $p<0.0001$, interaction: $p<0.0001$; n=4-7). **(F)** No difference was observed in smooth muscle reactivity (HTN: $p=0.9702$, time: $p=.1981$, interaction: $p=.6479$; n=4-7). **(G-I)** DOCA induced cognitive impairment assessed by **(G)** percent time exploring a novel object (HTN: $p<0.0001$, time: $p<0.0001$, interaction: 0.0012; n=5-11), **(H)** time in target quadrant (TQ) during Barnes maze probe trial (HTN: $p<0.0001$, time: $p=0.6531$, interaction: 0.7123; n=13), and **(I)** nest building assessed on the Deacon score scale (HTN: $p=0.0125$, time: $p=0.0069$, interaction: p=0093; n=10-20). Representative images of a single mouse from each group are shown for novel object recognition, Barnes maze probe trial, and nest building. All intergroup differences analyzed by two-way ANOVA and Bonferroni's multiple comparison test. Data are shown as mean $\pm$ SEM.

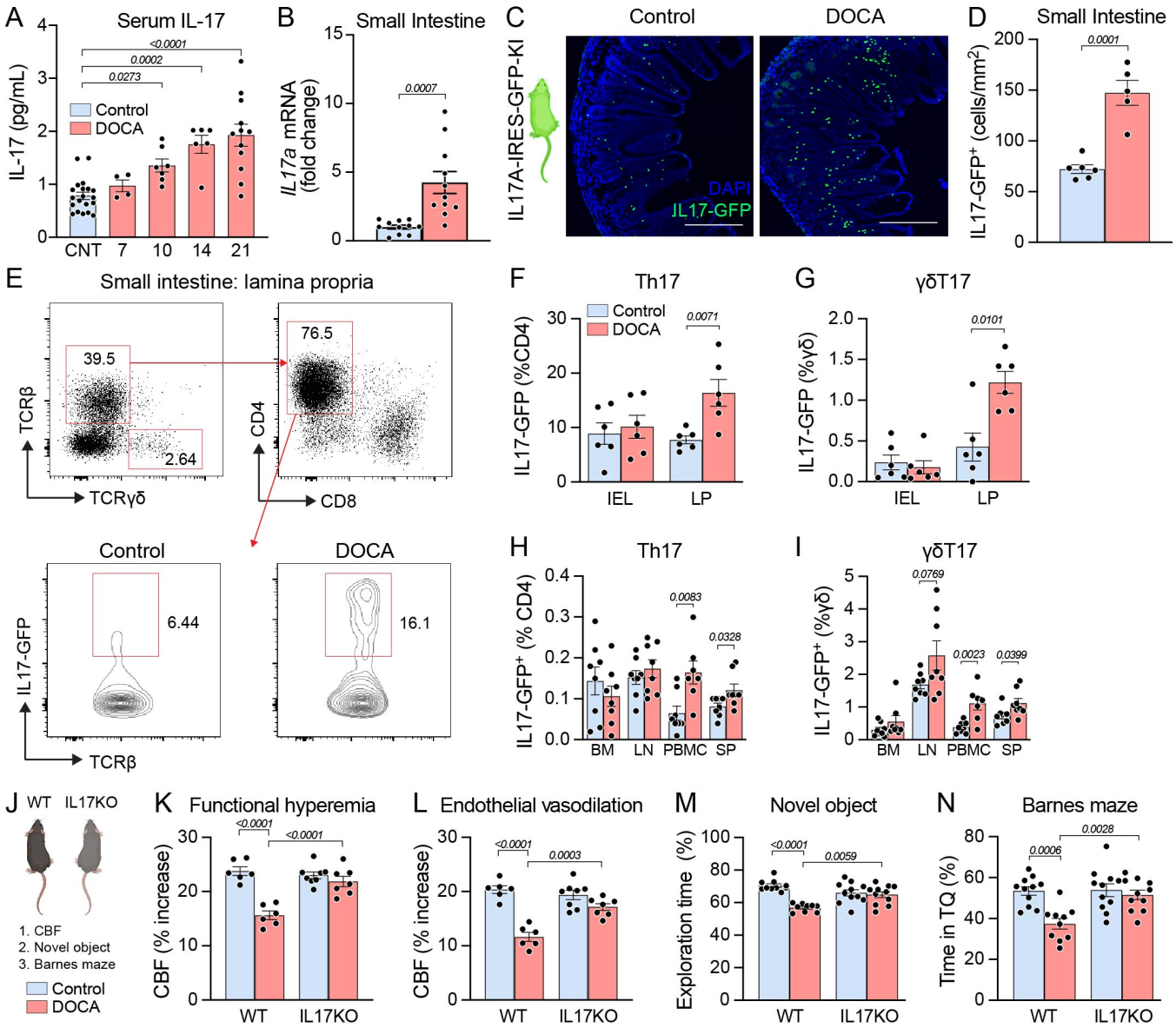

Figure 2. The neurovascular and cognitive impairment induced by DOCA is mediated by IL-17. **(A)** Serum IL-17 is elevated in DOCA HTN starting at 10 days ($p<0.0001$; one-way ANOVA and Bonferroni's multiple comparison test; n=5-18 as shown). **(B)** 21 days of DOCA-salt increased *Il17a* mRNA (unpaired two-tailed t-test, n=11) as well as **(C-D)** IL17-GFP cells in the small intestine. (unpaired two-tailed t-test); Scale bar: 300μm. **(E)** By flow cytometry, these cells were identified to be **(F)** Th17 and **(G)** γδT17 in the lamina propria (LP) not intraepithelial lymphocytes (IEL) (unpaired two-tailed t-test, n=6). **(H-I)** Th17 and γδT17 were also expanded in peripheral blood mononuclear cells (PBMC) and spleen (SP), but not in the bone marrow (BM) or lymph nodes (LN) (unpaired two-tailed t-test per organ, n=7-8). **(J-N)** IL-17 deficient mice (KO) did not exhibit an attenuation in functional hyperemia (HTN: $p<0.0001$, genotype: $p=0.0024$, interaction: $p=0.0002$; two-way ANOVA and Bonferroni's multiple comparison test; n=6-8) and endothelial vasodilation (HTN: $p<0.0001$, genotype: $p=0.0079$, interaction: $p=0.0004$; two-way ANOVA and Bonferroni's multiple comparison test; n=6-8), and no deficits were observed in either novel object (HTN: $p<0.0001$, genotype: $p=2603$, interaction: $p=0.0003$; two-way ANOVA and Bonferroni's multiple comparison test; n=9-11) or Barnes maze tests (HTN: $p=0.001$, genotype: $p=0.0076$, interaction: $p=0.0114$; two-way ANOVA and Bonferroni's multiple comparison test; n=9-11). Data are shown as mean ± SEM.

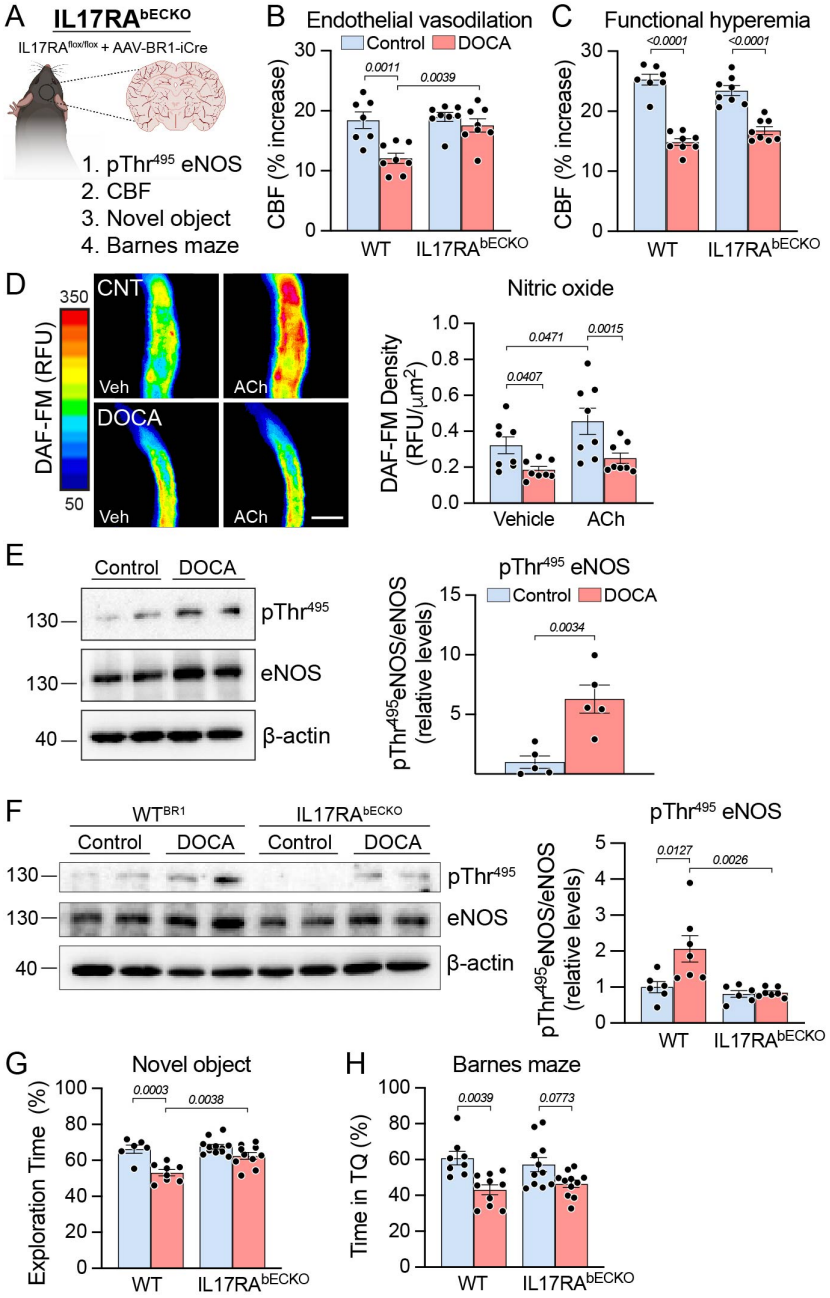

Figure 3. IL-17 impairs endothelial vasodilation by downregulating NO bioavailability via endothelial IL-17 receptors. (A-C) IL17RA brain endothelial cell knockout (IL17RAb^{ECKO}) mice are protected from the impairment in endothelial vasodilation (HTN: p=0.0007, genotype: p=0.0067, interaction: p=0.0223; two-way ANOVA and Bonferroni's multiple comparison test; n=7-8) but not the impairment in functional hyperemia induced by DOCA (HTN: p<0.0001, genotype: p=0.9446, interaction: p=0.0161; two-way ANOVA and Bonferroni's multiple comparison test; n=7-8). **(D)** Resting and ACh-induced endothelial NO production was attenuated in DOCA cerebral microvascular preparations (p<0.0001, repeated measured one-way ANOVA and Tukey's multiple comparison test; n=8). Scale bar: 50μm. **(E-F)** eNOS inhibitory phosphorylation was increased by DOCA in WT mice (unpaired two-tailed t-test), an effect suppressed in IL-17RAb^{ECKO} (HTN: p=0.0185, genotype: p=0.0037, interaction: p=0.0266; two-way ANOVA and Bonferroni's multiple comparison test; n=5-7). **(G-H)** IL17RAb^{ECKO} displayed cognitive improvement only at novel object recognition (HTN: p<0.0001, genotype: p=0.0061, interaction: p=0.0338; two-way ANOVA and Tukey's multiple comparison test; n=6-12), not the Barnes maze (HTN: p<0.0001, genotype: p=0.9599, interaction: p=0.2875; two-way ANOVA and Tukey's multiple comparison test; n=6-12). Data are shown as mean ± SEM.

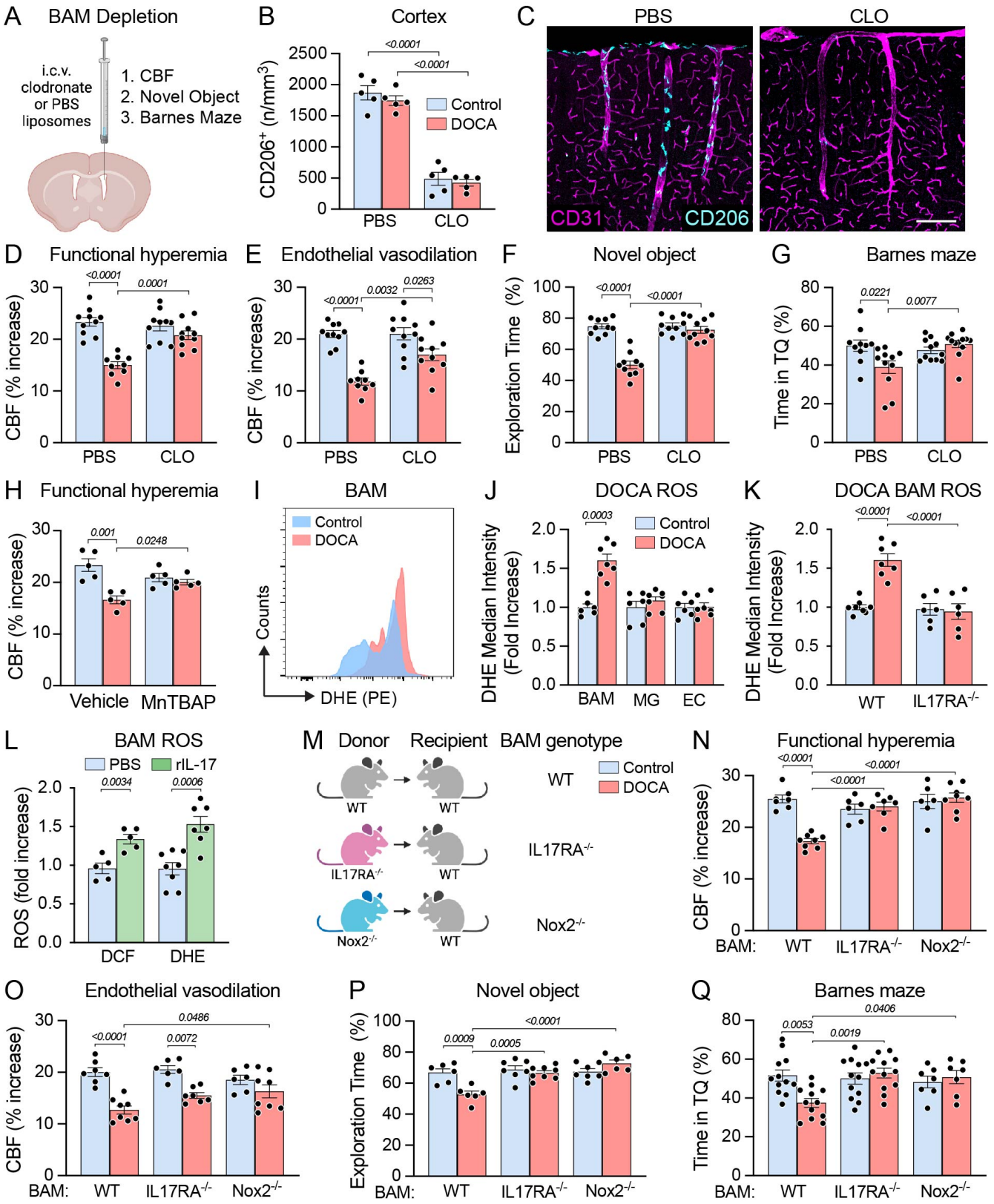

Figure 4. IL-17 impairs functional hyperemia via enhanced free radical production mediated by IL-17RA in BAM. (A-C) Brain associated macrophage (BAM), including perivascular and leptomeningeal macrophages, were depleted by 80% 21 days after intracerebroventricular delivery of liposome-encapsulated clodronate depletes (HTN: p=0.3156, liposomes: p=<0.0001, interaction: p=0.7304; two-way ANOVA and Tukey's multiple comparison test; n=5). Scale bar: 150μm. **(D-G)** BAM

depletion normalized functional hyperemia (HTN: $p<0.0001$, liposomes: $p=0.0050$, interaction: $p=0.0004$; two-way ANOVA and Tukey's multiple comparison test; n=9-10) and partially improved endothelial vasoactivity (HTN: $p<0.0001$, liposomes: $p=0.01$, interaction: $p=0.0112$, two-way ANOVA and Tukey's multiple comparison test; n=9-10) while also improving cognitive function assessed by novel object recognition (HTN: $p<0.0001$, liposomes: $p<0.0001$, interaction: $p<0.0001$, two-way ANOVA and Bonferroni's multiple comparison test; n=10) and Barnes maze (HTN: $p=0.1240$, liposomes: $p=0.0648$, interaction: $p=0.0062$, two-way ANOVA and Bonferroni's multiple comparison test; n=10-12). **(H)** Neocortical application of the ROS scavenger MnTBAP rescued the impairment of functional hyperemia in DOCA-salt ($p=0.0017$, repeated measures one-way ANOVA with Tukey's multiple comparison test, n=5). **(I-K)** The increased ROS production in BAM induced by DOCA-salt (HTN: $p=0.0033$, cell type: $p<0.0001$, interaction: $p<0.0001$; two-way repeated measures ANOVA with Bonferroni's multiple comparisons test; n=6-7) is prevented in IL-17RA deficient mice (HTN: $p=0.0006$, genotype: $p<0.0001$, interaction: $p=0.0002$; two-way ANOVA with Bonferroni's multiple comparison test; n=6-8). **(L)** Recombinant IL-17 increased ROS production in BAM (unpaired two-tailed t-test per ROS indicator, n=5-8). **(M-Q)** Deletion of either IL-17RA or Nox2 from BAM in BM chimeras prevented the impairment of functional hyperemia in full (HTN: $p=0.0030$, BAM genotype: $p=0.0003$, interaction: $p<0.0001$; two-way ANOVA with Tukey's multiple comparison test; n=6-8), improved endothelial vasoactivity (HTN: $p<0.0001$, BAM genotype: $p=0.1898$, interaction: $p=0.0248$; two-way ANOVA with Tukey's multiple comparison test; n=6-8), as well as cognitive function (novel object HTN: $p=0.0392$, BAM genotype: $p<0.0001$; interaction: $p=0.0004$; Barnes HTN: $p=0.2287$, BAM genotype: $p=0.0362$, interaction: $p=0.0040$; two-way ANOVA with Tukey's multiple comparison test; n=6-8). Data are shown as mean $\pm$ SEM.

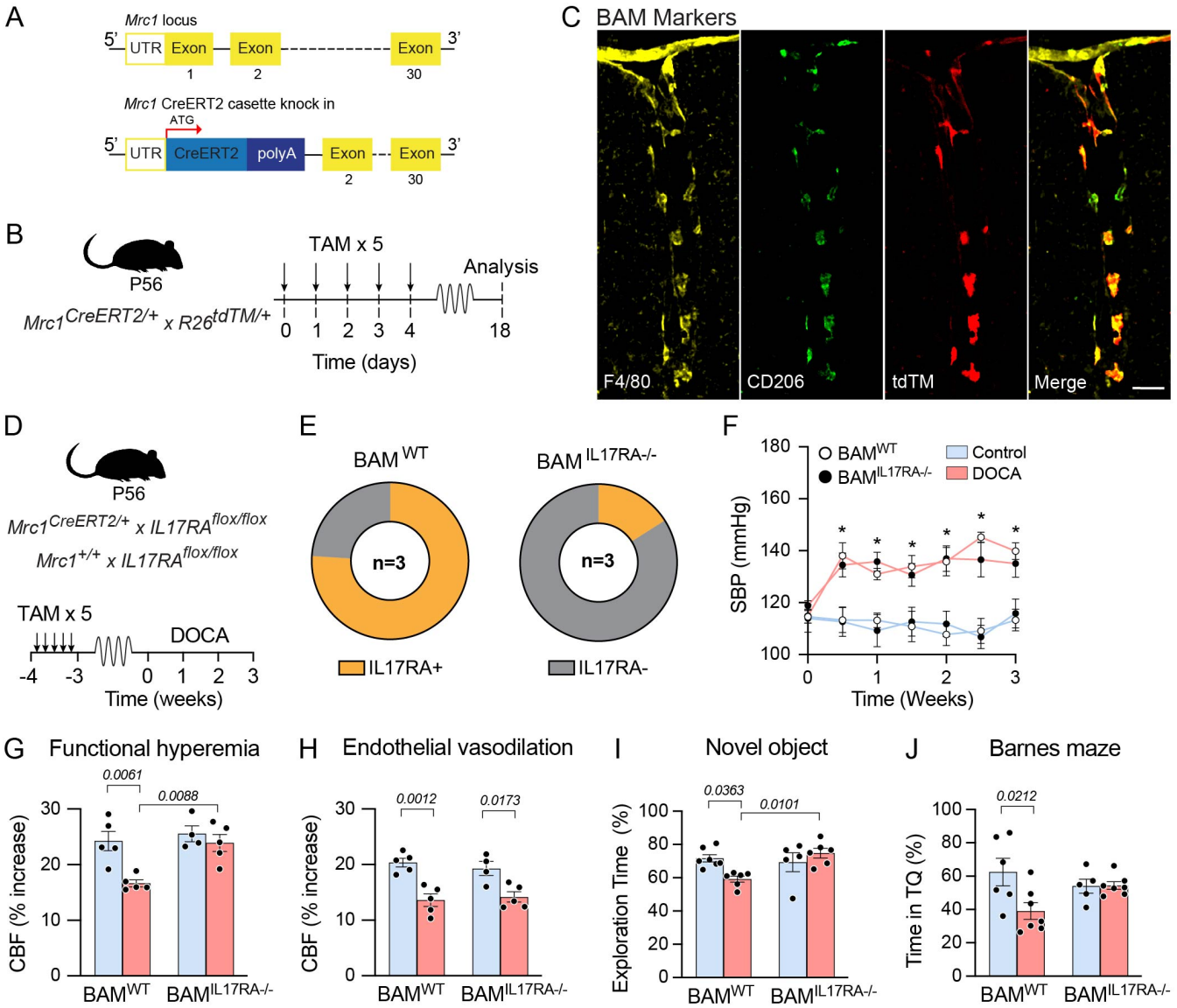

Figure 5. IL17-RA deletion in BAM improves functional hyperemia and cognitive function in DOCA-salt. (A) CreERT2 cassette was introduced into the endogenous Mrc1 locus. **(B)** These mice were crossed with the Ai14 TdTomato reporter mice, and **(C)** showed TdTM expression in BAM. Scale bar: 50μm. **(D)** $Mrc1^{CreERT2}$ mice were crossed with $IL17\text{-}RA^{flox/flox}$ to generate $BAM^{IL17RA-/-}$. **(E)** IL17RA expression was reduced by 78.9% in $BAM^{IL17RA-/-}$ compared to BAM^{WT} mice. (n=3 mice/group; 50 BAM per mouse; p<0.0001, two-way ANOVA with Bonferroni's multiple comparisons test). **(F)** Blood pressure under control and DOCA-salt conditions was not altered in BAM^{WT} or $BAM^{IL17RA-/-}$ mice (two-way repeated measures ANOVA with Tukey's multiple comparisons test). **(F-G)** IL17-RA deletion in BAM restored functional hyperemia (HTN: p=0.0048, genotype: p=0.0080, interaction: p=0.0499; two-way ANOVA with Bonferroni's multiple comparison test; n=4-5) without improving endothelial vasodilation (HTN: p<0.001, genotype: p=0.8120, interaction: p=0.4368; two-way ANOVA with Bonferroni's multiple comparison test; n=4-5), and **(H-I)** rescued cognitive function after 21 days of DOCA-salt (novel object HTN: p=0.2638, genotype: p=0.0460; interaction: p=0.0100; Barnes HTN: p=0.0427, genotype: p=0.5297, interaction: p=0.0365; two-way ANOVA with Tukey's multiple comparison test; n=5-7). Data are shown as mean ± SEM.

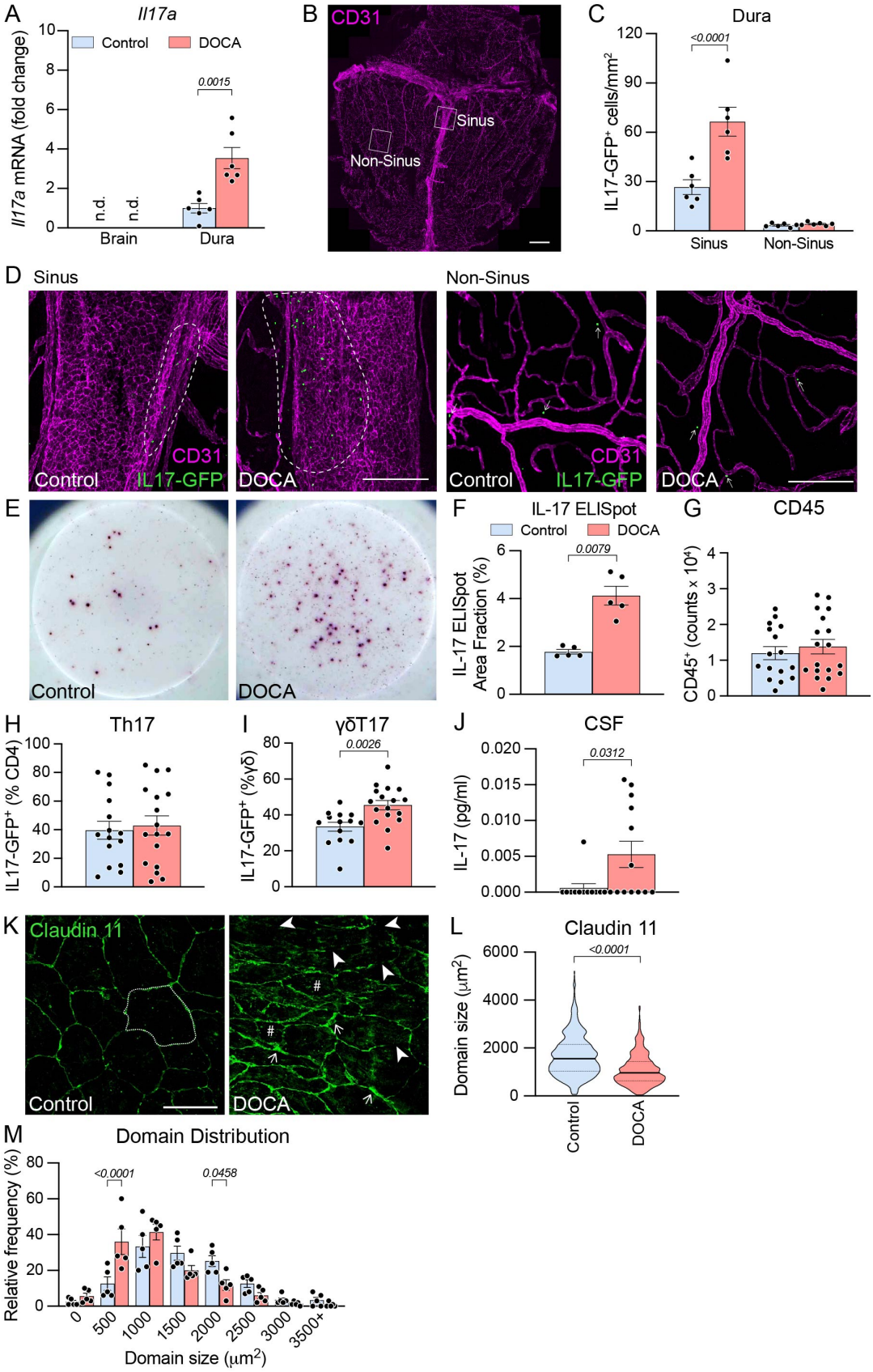

Figure 6. Salt-sensitive hypertension increases IL17-producing T cells located in the dura mater. **(A)** *Il17a* mRNA was not observed in the brain parenchyma, but it was detected in dura mater of control mice and was markedly increased by DOCA-salt (unpaired two-tailed t-test; n=6). **(B)** Dura whole

mount stained with CD31 (magenta). Scale bar: 1mm. **(C)** DOCA-salt treatment led to a significant increase in IL17-GFP+ cells in the vicinity of the venous sinuses (HTN: $p=0.0017$, Sinus: $p<0.0001$, interaction: $p=0.0034$; two-way repeated measures ANOVA with Bonferroni's multiple comparison test; n=6). **(D)** Representative images of control and DOCA sinus and non-sinus regions. Analysis shown in 6C. **(E-F)** Dural isolated cells secrete IL-17, and this response is increased in DOCA-salt mice (unpaired two-tailed t-test; n=5). **(G)** DOCA-salt does not change the total number of CD45 immune cells isolated from dura. (**H-I)** DOCA-salt increases the percentage of $\gamma\delta$T17 cells but no difference in Th17 cells (unpaired two-tailed t-test; n=14-17 mice). **(J)** IL-17 detection was increased in the cerebrospinal fluid (CSF) after 21 days of DOCA-salt (Wilcoxon signed-rank test, n=12-13). **(K)** Arachnoid barrier integrity was assessed by the arachnoid barrier tight junction marker Claudin-11. Arrowheads indicate discontinuous tight junctions, # indicates reduced arachnoid domain size, and thin arrows indicate altered tight junction morphology. (**L-M**) Arachnoid barrier domain size (Kolmogrov-Smirnov test; n=616-663 domains [5 mice, 10 images per mouse, all domains per image quantified]) and distribution was altered by DOCA-salt (HTN: $p=0.9880$, domain size bin: $p<0.0001$; interaction: $p<0.0001$; two-way ANOVA with Bonferroni's multiple comparison test). Data are shown as mean $\pm$ SEM.

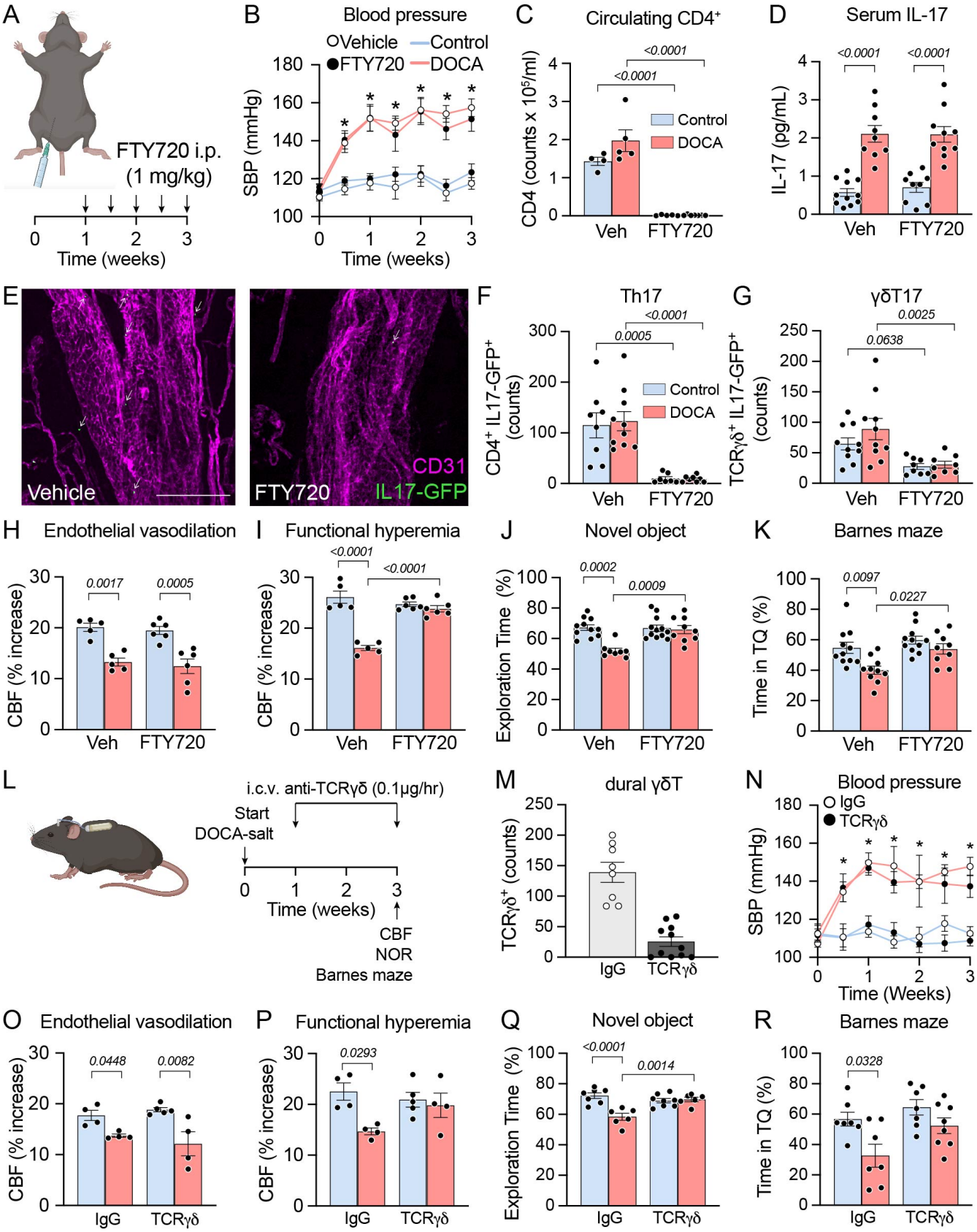

Figure 7. Cognitive impairment in salt-sensitive hypertension is driven by meningeal IL17-producing T cells. (A-B) FTY720 was administered from day 7 through day 21 of DOCA-salt and did not affect the increase in systolic blood pressure (treatment: $p<0.0001$, time: $p<0.0001$, interaction:

p=0.0182; two-way repeated measures ANOVA with Tukey's multiple comparison test; n=5-8). **(C-D)** FTY720 reduces circulating CD4 T cells (HTN: p=0.0705, treatment: p<0.0001, interaction: p=0.0737; two-way ANOVA with Tukey's multiple comparison test; n=4-7), without affecting the elevation in serum IL-17 in DOCA-salt (HTN: p<0.0001, treatment: p=0.7200, interaction: p=0.6622; two-way ANOVA with Tukey's multiple comparison test; n=9-11). **(E-G)** FTY720 reduced IL17-GFP cells in the meninges, including both Th17 (HTN: p=0.8358, treatment: p<0.0001, interaction: p=0.7848; two-way ANOVA with Bonferroni's multiple comparison test; n=8-10) and γδT17 (HTN: p=0.2517, treatment: p=0.0003, interaction: p=0.3639; two-way ANOVA with Bonferroni's multiple comparison test; n=8-10). **(H-K)** FTY did not improve endothelial vasoactivity (HTN: p<0.0001, treatment: p=0.4839, interaction: p=0.9293; two-way ANOVA with Bonferroni's multiple comparison test; n=5-6), but completely restored functional hyperemia (HTN: p<0.0001, treatment: p=0.0004, interaction: p<0.0001; two-way ANOVA with Bonferroni's multiple comparison test; n=5-6), as well as improved cognitive function (novel object HTN: p=0.0007, treatment: p=0.0037; interaction: p=0.0023; Barnes HTN: p=0.0023, treatment: p=0.0045, interaction: p=0.1695; two-way ANOVA with Tukey's multiple comparison test; n=8-12). **(L)** anti-TCRgd antibody was delivered i.c.v. from day 7 to 21 of DOCA-salt. **(M)** anti-TCRgd antibody treatment reduced gdT cells in the dura (p<0.0001, two-tailed unpaired t-test). **(N)** anti-TCRgd antibody did not alter the blood pressure response to DOCA-salt (two-way repeated measures ANOVA with Tukey's multiple comparisons test). **(O-R)** Dura gdT cell depletion did not restore endothelial vasodilation (HTN: p=0.0008, treatment: p=0.8541, interaction: p=0.2935; two-way ANOVA with Tukey's multiple comparison test; n=4-5), but was associated with improved functional hyperemia (HTN: p=0.0190, treatment: p=0.3072, interaction: p=0.0655; two-way ANOVA with Tukey's multiple comparison test; n=4-5) and cognitive function (novel object HTN: p=0.0012, treatment: p=0.0323; interaction: p=0.0004; Barnes HTN: p=0.0040, treatment: p=0.0229, interaction: p=0.3002; two-way ANOVA with Tukey's multiple comparison test; n=6-8). Data are shown as mean ± SEM.

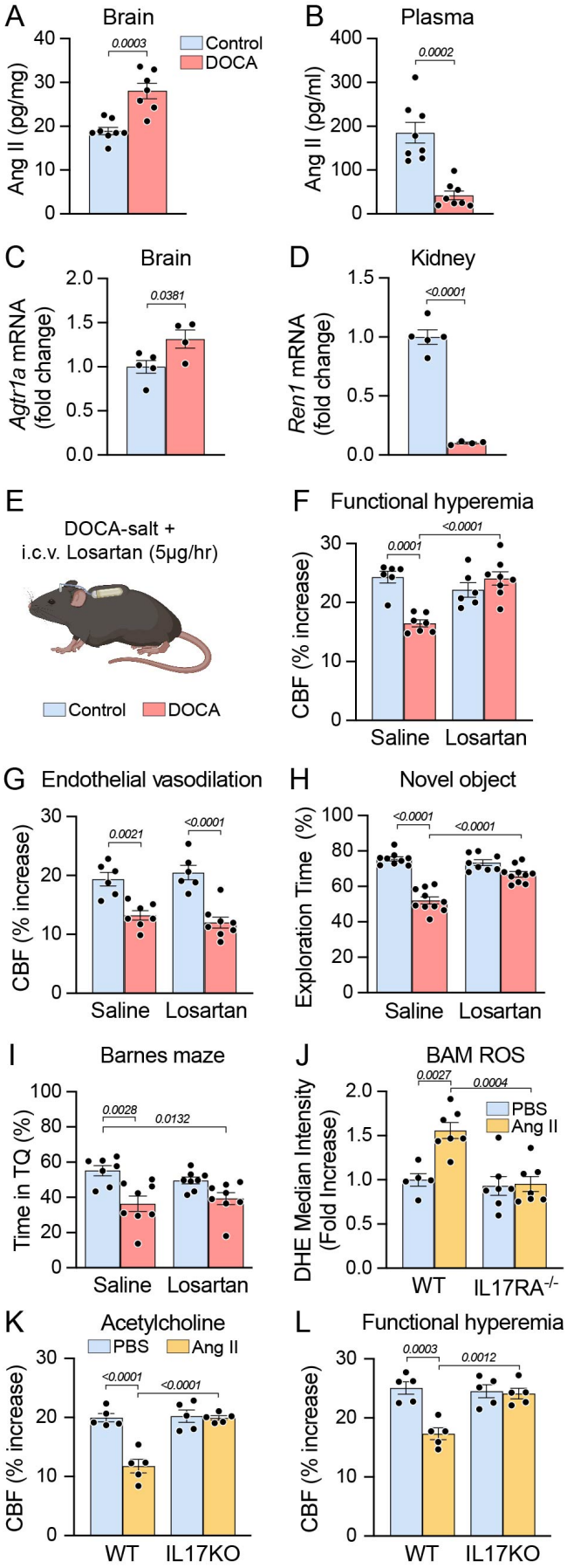

Figure 8. The contribution of Ang II to the cerebrovascular dysfunction in DOCA-salt depends on IL-17 signaling. (A-B) DOCA-salt treatment elevated Ang II levels in brain and reduced it in the circulation (unpaired two-tailed t-test; n=7-8). **(C-D)** DOCA-salt upregulates brain *Agtr1a* and downregulates kidney renin (unpaired two-tailed t-test; n=4-5). **(E-G)** Central AT1R blockade with i.c.v. losartan restored functional hyperemia (HTN: p=0.0088, treatment: p=0.0148, interaction: p<0.0001; two-way ANOVA with Bonferroni's multiple comparison test; n=6-8), but did not improve endothelium-dependent vasodilation (HTN: p<0.0001, treatment: p=0.9604, interaction: p=0.2642; two-way ANOVA with Bonferroni's multiple comparison test; n=6-8). **(H-I)** Central AT1R blockade improved novel object recognition (HTN: p<0.0001, treatment: p=0.0005, interaction: p<0.0001; two-way ANOVA with Tukey's multiple comparison test; n=8-10), but did not improve Barnes maze (HTN: p=0.0002; treatment: p=0.6968, interaction: p=0.2113; two-way ANOVA with Tukey's multiple comparison test; n=7-8). **(J)** Ang II stimulation increased ROS production in WT but not IL17RA$^{-/-}$ BAM (genotype: p=0.0015; treatment: p=0.0050, interaction: p=0.0087; two-way ANOVA with Tukey's multiple comparison test; n=5-7). **(K-L)** Neocortical application of Ang II impaired endothelial vasoactivity (genotype: p=0.0029; treatment: p=0.0003, interaction: p=0.0004; two-way repeated measures ANOVA with Bonferroni's multiple comparison test; n=5) and induced neurovascular dysfunction (genotype: p=0.0374; treatment: p=0.0003, interaction: p=0.0005; two-way repeated measures ANOVA with Bonferroni's multiple comparison test; n=5) in WT but not IL17KO mice. Data are shown as mean ± SEM.